Interference effects in the decay of resonance states in three-body Coulomb systems

Oleg I. Tolstikhin,[1,*] Inga Yu. Tolstikhina,[2] and Chusei Namba[3]
[1]*Russian Research Center ''Kurchatov Institute,'' Kurchatov Square 1, Moscow 123182, Russia*
[2]*P. N. Lebedev Physical Institute, Leninsky Prospect 53, Moscow 117924, Russia*
[3]*National Institute for Fusion Science, Toki, 509-5292, Japan*
(Received 29 July 1999)

The lowest $^1S^e$ resonance state in a family of symmetric three-body Coulomb systems is systematically studied as a function of the mass-ratio M for the constituting particles. The Siegert pseudostate method for calculating resonances is described and accurate results obtained by this method for the resonance position $\mathcal{E}(M)$ and width $\Gamma(M)$ in the interval $0 \leqslant M \leqslant 30$ are reported. The principal finding of these calculations is that the function $\Gamma(M)$ oscillates, almost vanishing for certain values of M, which indicates the existence of an interference mechanism in the resonance decay dynamics. To clarify this mechanism, a simplified model obtained from the three-body Coulomb problem in the limit $M \to \infty$ is analyzed. This analysis extends the range of M up to $M = 300$ and confirms that $\Gamma(M)$ continues to oscillate with an increasing period and decreasing envelope as M grows. Simultaneously it points to semiclassical theory as an appropriate framework for explaining the oscillations. On the basis of Demkov's construction, the oscillations are interpreted as a result of interference between two paths of the resonance decay on the Riemann surface of adiabatic potential energy, i.e., as a manifestation of the Stueckelberg phase. It is shown that the implications of this interpretation for the period and envelope of the oscillations of $\Gamma(M)$ agree excellently with the calculated results.
[S1050-2947(99)09912-6]

PACS number(s): 34.10.+x, 31.15.Ja, 36.10.−k

I. INTRODUCTION

Resonance phenomena have always attracted much interest among theorists, and this is understandable. On the one hand, resonances occupy an intermediate position between bound states and true continuum scattering processes. Indeed, like bound states resonances are described by solutions of certain (Siegert) eigenvalue problem formulated in terms of the Hamiltonian of the system, and in contrast to scattering processes they are characterized by just two observable parameters, the resonance position $\mathcal{E}$ and width Γ defined by the complex energy eigenvalue

$$E = \mathcal{E} - i\Gamma/2. \tag{1}$$

At the same time, in contrast to bound states, resonance eigenfunctions are not localized in a restricted region of configuration space but like continuous energy wave functions extend to infinity incorporating the influence of asymptotic boundary conditions. Thus resonances convey a more informative message about the system's dynamics than bound states while remaining a simpler object for study than continuum processes. On the other hand, there are features peculiar to resonances which justifies placing them into a separate chapter of scattering theory. The very existence of resonances rests on a subtle balance in the energy exchange between different degrees of freedom in the system, and the two basic mechanisms of their decay, namely, the nonadiabatic transitions and tunneling, belong to the most complicated issues of quantum mechanics. All this makes the physics of resonances rich in content and keeps motivating researchers.

The existing methods of resonance calculations can be classified according to whether the energy E in the Schrödinger equation is treated as real or complex. In the different variants of scattering calculations, Kohn variational and stabilization methods, one stays on real energy axis. Resonances in this approach are understood and sought as sharp peaks in the energy dependence of the scattering matrix or some other calculated quantity, and the resonance parameters $\mathcal{E}$ and Γ are extracted indirectly via a fitting procedure. Complex variational calculations and complex rotation methods are based on the definition of resonances as the solutions to the Schrödinger equation satisfying the outgoing wave boundary conditions. The consistent implementation of this approach leads one to an eigenvalue problem which in order to be solved requires considering complex energies. Such eigenvalue problem was first formulated by Siegert [1] and its solutions are now known as Siegert states. The physical resonances are represented by those of the Siegert states whose eigenvalues lie close to real energy axis, and the resonance parameters can be obtained directly from the eigenvalues via Eq. (1). Finally, there exist mixed approaches such as perturbation theory and Feshbach formalism where the resonance eigenvalue is firstly assumed to be purely real and only on the subsequent stage of calculations attains a small complex correction characterizing the resonance shift and width. Each of these approaches has its own merits as well as demerits; they all have been demonstrated to be capable of producing accurate numerical results and the choice between them in any particular situation is a matter of computational convenience or even personal preference. In our opinion, the

*Electronic address: oleg@muon.imp.kiae.ru

 ©1999 The American Physical Society

approach based on the Siegert eigenvalue problem has conceptual advantages and conceals yet undeveloped potentialities. The point is that the set of Siegert states besides resonances includes also bound and antibound (virtual) states and possesses certain completeness properties that qualify it as a basis suitable for expanding the continuum. This opens a possibility to reformulate scattering theory in terms of a purely discrete set of states — a long standing ambition whose numerical implementation, however, meets serious difficulties and still remains an open problem. Perhaps a solution to this problem can be found within the Siegert pseudostate (SPS) formulation recently proposed in [2] and thoroughly developed for the one-channel case in [3]. The reader is referred to these papers for a more detailed discussion and extensive bibliography on the subject, while for the present purposes it is sufficient to note that as a method for calculating resonances the SPS formulation has been shown to provide the highest precision in all studied cases, which includes a large number of one-dimensional models [3] and several realistic three-body Coulomb systems [2].

This work continues a series of studies on the three-body Coulomb problem [4–7,2,8,9] whose common goal is to advance the field via the synergism of new mathematical methods and modern computational resources. Here, we apply the SPS formulation to the systematic study of the lowest resonance in a family of symmetric three-body Coulomb systems as a function of the ratio M of the masses of the constituting particles. The atomic limit $M\to 0$ in this family is represented by the two-electron atomic ion H^-. Understanding of interelectron correlation in two-electron atoms is regarded as one of the most fundamental problems in atomic physics. It is well known what a strong impetus for the theory was given by the first experimental observation of resonances in helium [10], and nowadays experimental studies of high-lying doubly excited states in two-electron atoms, which became possible due to significant enhancement of the spectral brightness of modern light sources [11], again challenge theorists. A prototype system in the molecular limit $M\to\infty$ of the mass-ratio spectrum is the diatomic molecular ion H_2^+. This system is a counterpart of H^-, with protons and electrons being interchanged. Both systems are abundant in hydrogenic plasmas and seem to be equally available for laboratory observations. However H_2^+ is still much less studied experimentally and, on the theoretical side, fewer words are heard about *interproton* correlation in H_2^+ than about *interelectron* correlation in H^- although, in our opinion, the former is a no less fundamental problem than the latter. We believe the situation will change when spectroscopic studies of H_2^+ and its isotopomers will be extended from the ground [12] to excited electronic states, and counterparts of the resonances that have played so important role in studying two-electron atoms will be observed in these molecular systems. In between these two extreme limits of the mass-ratio M there exist many more exotic three-body Coulomb systems. In this work, concentrating on one particular resonance state and tracing it as a function of M from H^- to H_2^+, we wish to discuss a very general mechanism which reveals itself in the dynamics of all these vastly different systems.

The paper consists of three parts. In Sec. II we report accurate results for the resonance position $\mathcal{E}(M)$ and width $\Gamma(M)$ as functions of the mass-ratio M in the interval $0 \leqslant M \leqslant 30$. The principal and rather unexpected finding here is that the function $\Gamma(M)$ oscillates, almost vanishing at certain values of M. In order to provide convincing evidence for the correctness of this numerical result we give a detailed account of the hyperspherical elliptic — slow/smooth variable discretization (HSE-SVD) representation [4–6] and the SPS method [2,3] used in the calculations. Accuracy of the calculations matters, so a special effort is paid to demonstrating convergence of the results on the example of several realistic three-body Coulomb systems that fall in the considered interval of M. Section III serves as a bridge between heavy calculations reported in Sec. II and qualitative interpretation of their results to be given in Sec. IV. Here, we discuss a simplified model obtained from the three-body Coulomb problem in the limit $M\to\infty$. The perturbation analysis of this model extends the considered interval of the mass-ratio up to $M=300$ and qualitatively confirms the results of Sec. II. Meanwhile, this model depends on M in a more transparent manner which makes it clear that an explanation of the oscillations of $\Gamma(M)$ should be sought in terms of semiclassical theory. In Sec. IV, without actually developing the semiclassical analysis of the problem, on the basis of Demkov's construction we show that the major features of the calculated dependence $\Gamma(M)$ agree excellently with that dictated by semiclassical theory. This leads us to the interpretation of the oscillations of $\Gamma(M)$ as a result of interference between two paths of the decay of the resonance state on the Riemann surface of adiabatic potential energy, i.e., as a manifestation of the Stueckelberg phase. Summary of the results and a brief discussion of possible implications of this interference mechanism conclude the paper in Sec. V.

II. ACCURATE CALCULATIONS BY THE SIEGERT PSEUDOSTATE METHOD

Let us begin by specifying more precisely the family of systems and the state to be dealt with in the following. Consider a system of three Coulomb point particles two of which are identical and the third one having a charge of the same absolute value but of opposite sign. Let $m_1=m_2$ and m_3 be masses and $Z_1=Z_2=-Z_3$ be charges of the particles. It is convenient to introduce modified atomic units (to be abbreviated as m.a.u.) defined by $m_3=|Z_3|=\hbar=1$; this system of units will be used throughout the paper unless explicitly stated otherwise. Then the mass-ratio $M\equiv m_1/m_3=m_2/m_3$ is the only dimensionless parameter characterizing the system. In Table I we list several realistic three-body Coulomb systems of this type. Some of them are routine objects of experimental studies while some others have not been detected in a laboratory as yet. The list includes systems composed mostly of stable particles and only muons $\mu^\pm$ are unstable; it can be extended if we admit more exotic unstable particles such as pions $\pi^\pm$, kaons $K^\pm$, etc., as constituents. The parameter M in these systems varies over more than 7 orders of magnitude which produces a tremendous change of the physical properties on the way from two-electron atoms to diatomic molecules. But what is more important in the present context is that the real physical systems are rather densely distributed over this interval of M. So it seems to be

TABLE I. Some realistic three-body Coulomb systems belonging to the family considered in this work. These systems are characterized by a single dimensionless parameter M giving the ratio of the masses of the constituting particles. The values of M were obtained using the particles' masses taken from [13].

System	M	System	M
$eet(\mathrm{T}^-)$	$0.181\,920\,00\times10^{-3}$	$dd\bar{p}$	1.999 0075
$eed(\mathrm{D}^-)$	$0.272\,443\,71\times10^{-3}$	$tt\bar{p}$	2.993 7170
$eep(\mathrm{H}^-)$	$0.544\,617\,01\times10^{-3}$	$pp\mu$	8.880 2445
$ee\mu^+$	$0.483\,633\,22\times10^{-2}$	$dd\mu$	17.751 675
$\mu\mu t$	$0.376\,152\,83\times10^{-1}$	$tt\mu$	26.584 939
$\mu\mu d$	$0.563\,327\,12\times10^{-1}$	$\mu\mu e^+$	206.768 26
$\mu\mu p$	0.112 609 51	$ppe(\mathrm{H}_2^+)$	1836.152 7
$\overline{ppt}$	0.334 032 91	$dde(\mathrm{D}_2^+)$	3670.483 0
$\overline{ppd}$	0.500 248 25	$tte(\mathrm{T}_2^+)$	5496.921 6
$eee^+(\mathrm{Ps}^-)$	1		

sensible instead of focusing on individual systems to study *continuous* variation of their physical properties as a function of M, and this is the approach adopted in this work. This defines the systems and now we turn to the state. We shall consider the lowest resonance state of the $^1S^e$ symmetry, where S stands for zero total angular momentum, $L=0$; 1 indicates that the state is symmetric under permutation of the identical particles, by analogy with two-electron atoms where this notation would mean ''singlet''; and e stands for even parity indicating that the state is symmetric under the inversion of space, which is the only option for an S state. In other words, we shall consider the state whose approximate classification changes, as M increases, from $2s^2$ in terms of the independent electron quantum numbers in the atomic limit $M\to0$ to $3d\sigma_g v=0$ in terms of the united atom quantum numbers defining the electronic state and the vibrational quantum number defining the internuclear motion in the molecular limit $M\to\infty$. An alternative classification of this resonance state in terms of hyperspherical elliptic quantum numbers that applies universally throughout the whole range of M is discussed below.

In this section, first we give a summary of the HSE-SVD representation specifically for the one-parametric family of symmetric three-body Coulomb systems defined above, then we reduce the problem of calculating resonances in such systems to an algebraic eigenvalue problem for Siegert pseudostates, and finally we present our numerical results.

A. Hyperspherical elliptic—slow/smooth variable discretization (HSE-SVD) representation

The Schrödinger equation for a three-body system after the separation of the center-of-mass motion for states with zero total angular momentum of interest here contains three independent variables. A common strategy in solving such multidimensional equations numerically consists in expanding the solution in terms of some set of basis functions. The choice of the basis and the particular structure of the expansion defines a representation. This is the point where the matters of physics and calculation meet in the sense that the more *a priori* knowledge about the system is built into the representation the more numerically efficient it is. In this work we use the HSE-SVD representation introduced in [4–6]. This representation has proven to be very efficient and accurate for calculating bound states, resonances, elastic and rearrangement scattering processes in various three-body Coulomb systems [4–7,2,8,9] and recently it has been extended to studying atom-diatom chemical reactions [14,15]. However, in spite of numerous applications a consistent account of this approach and its potentialities still waits to be written. Here, we summarize necessary details specifically for systems of the type defined above.

The HSE-SVD representation rests on two pillars: a good coordinate system which reveals an approximate symmetry of the three-body Coulomb problem and the idea of adiabatic separability between hyperradius and hyperangular variables for systems with Coulomb interactions. We begin with the coordinate system. Let $\mathbf{r}_i$, $i=1,2,3$, give the positions of the particles in the center-of-mass frame, with the particles 1 and 2 being identical, and let $r_{ij}=|\mathbf{r}_i-\mathbf{r}_j|$ be the interparticle distances. Note that the vectors $\mathbf{r}_i$ are linear dependent,

$$M(\mathbf{r}_1+\mathbf{r}_2)+\mathbf{r}_3=0. \tag{2}$$

We introduce two sets of mass-scaled Jacobi coordinates:

$$\mathbf{x}_1=\sqrt{\frac{1+2M}{1+1/M}}\,\mathbf{r}_1, \quad \mathbf{y}_1=\frac{\mathbf{r}_3-\mathbf{r}_2}{\sqrt{1+1/M}}, \tag{3a}$$

$$\mathbf{x}_2=\sqrt{\frac{1+2M}{1+1/M}}\,\mathbf{r}_2, \quad \mathbf{y}_2=\frac{\mathbf{r}_1-\mathbf{r}_3}{\sqrt{1+1/M}}. \tag{3b}$$

These sets are related to each other by the Smith kinematic rotation [16]

$$\begin{pmatrix}\mathbf{x}_2\\ \mathbf{y}_2\end{pmatrix}=\begin{pmatrix}-\cos\gamma & -\sin\gamma\\ \sin\gamma & -\cos\gamma\end{pmatrix}\begin{pmatrix}\mathbf{x}_1\\ \mathbf{y}_1\end{pmatrix}, \tag{4}$$

where the rotation parameter γ is a function of M defined by

$$\tan\gamma=\frac{\sqrt{1+2M}}{M}, \quad 0\leqslant\gamma\leqslant\frac{\pi}{2}. \tag{5}$$

For each of the sets we introduce the corresponding hyperangle:

$$\tan(\chi_1/2)=\frac{y_1}{x_1}=\frac{r_{32}}{\sqrt{1+2M}r_1},\quad 0\leqslant\chi_1\leqslant\pi, \tag{6a}$$

$$\tan(\chi_2/2)=\frac{y_2}{x_2}=\frac{r_{13}}{\sqrt{1+2M}r_2},\quad 0\leqslant\chi_2\leqslant\pi. \tag{6b}$$

This definition differs from that of Delves [17] by the factor 1/2 which is due to Kuppermann [18]. Now we introduce the hyperradius

$$R=\sqrt{M(r_1^2+r_2^2)+r_3^2}=\sqrt{x_1^2+y_1^2}=\sqrt{x_2^2+y_2^2}, \tag{7}$$

$$0\leqslant R\leqslant\infty,$$

and the hyperspherical elliptic (HSE) coordinates [4]

$$\xi=\chi_1+\chi_2,\quad 2\gamma\leqslant\xi\leqslant 2\pi-2\gamma, \tag{8}$$

$$\eta=\chi_1-\chi_2,\quad -2\gamma\leqslant\eta\leqslant 2\gamma. \tag{9}$$

In terms of the variables R, ξ, and η the interparticle distances are expressed by

$$r_{32}=\sqrt{1+1/M}R\sin\left(\frac{\xi+\eta}{4}\right), \tag{10a}$$

$$r_{13}=\sqrt{1+1/M}R\sin\left(\frac{\xi-\eta}{4}\right), \tag{10b}$$

$$r_{21}=\frac{R}{\sqrt{M}}\sqrt{1+(1+1/M)\cos(\xi/2)\cos(\eta/2)}, \tag{10c}$$

thus R defines the size of the three-body triangle and (ξ,η) define its shape. As was demonstrated by previous experience [4–7,2,8,9], these variables are especially convenient for treating the three-body Coulomb problem and we shall use them as coordinates in configuration space. The surfaces of constant R are hyperspheres, and the hyperangular variables (ξ,η) define the position of a point on hypersphere. The volume element in these coordinates is given by

$$dV=\frac{\pi^2}{4\sin 2\gamma}R^5(\cos\eta-\cos\xi)dRd\xi d\eta, \tag{11}$$

where the normalization factor is chosen to yield $\pi^3/6$, i.e., the volume of unit sphere in 6D space, upon integrating over the region $R\leqslant 1$. The Schrödinger equation reads [4,5]

$$\left(-\frac{1}{2}\frac{\partial^2}{\partial R^2}+\frac{H_{\rm ad}(R)+15/8}{R^2}-E\right)R^{5/2}\Psi(R,\xi,\eta)=0, \tag{12}$$

where

$$H_{\rm ad}(R)=\tfrac{1}{2}\Lambda_0^2+RC(\xi,\eta) \tag{13}$$

is the hyperspherical adiabatic (HSA) Hamiltonian,

$$\Lambda_0^2=\frac{-16}{\cos\eta-\cos\xi}\times\left[\frac{\partial}{\partial\xi}(\cos 2\gamma-\cos\xi)\frac{\partial}{\partial\xi}+\frac{\partial}{\partial\eta}(\cos\eta-\cos 2\gamma)\frac{\partial}{\partial\eta}\right] \tag{14}$$

is the $L=0$ component of the Smith's grand angular momentum operator squared [19],

$$C(\xi,\eta)=\frac{-8\sin(\xi/4)\cos(\eta/4)}{\sqrt{1+1/M}}\frac{\cos(\xi/2)+\cos(\eta/2)}{\cos\eta-\cos\xi}+\frac{\sqrt{M}}{\sqrt{1+(1+1/M)\cos(\xi/2)\cos(\eta/2)}}, \tag{15}$$

is the effective charge representing the Coulomb potential energy

$$-\frac{1}{r_{32}}-\frac{1}{r_{13}}+\frac{1}{r_{21}}\equiv\frac{C(\xi,\eta)}{R}, \tag{16}$$

and E is the total energy of the system measured from the three-body breakup threshold. Note that the first term in Eq. (15) comprises both 1–3 and 2–3 attractive interparticle potentials, and the second term describes repulsion between the identical particles 1 and 2.

The boundary conditions for Eq. (12) consist of the condition of regularity of the wave function Ψ everywhere in configuration space and the physical asymptotic boundary condition at $R\to\infty$. The latter depends on the problem under consideration and for the present case will be specified in the next section. The former amounts to the requirement for Ψ to be regular at singular points of Eq. (12). These singularities must be properly treated in the numerical solution and it is important to realize their location. There are two types of singularities: those of the kinetic energy, which are singularities of the coordinate system, and those of the potential energy. The coordinate system (R,ξ,η) produces singularities at the points where the volume element (11) vanishes, that is at the origin $R=0$ and on four rays emanating from the origin and crossing hypersphere at $(\xi,\eta)=(2\gamma,\pm 2\gamma)$ and $(2\pi-2\gamma,\pm 2\gamma)$, i.e., at the apexes of the (ξ,η) rectangle defined by Eqs. (8) and (9). The Coulomb potential (16) is singular at the points of interparticle collisions, that is again at the origin $R=0$, which is the three-body coalescent point, and at the two-body coalescent points lying on three rays emanating from the origin and crossing hypersphere at $(\xi,\eta)=(2\gamma,-2\gamma)$ and $(2\gamma,+2\gamma)$ for the case of collisions in the pairs 2–3 and 1–3, respectively [the first term in Eq. (15)], and at $(\xi,\eta)=(2\pi-2\gamma,0)$ for collisions between the particles 1 and 2 [the second term in Eq. (15)]. The Coulomb singularities on the rays $(\xi,\eta)=(2\gamma,\pm 2\gamma)$ are attractive; these rays form the skeleton of the region of localization of

the wave function shaping its large-scale structure in configuration space and their coincidence with two of four singular rays of the coordinate system greatly facilitates the numerical solution. The third Coulomb singular ray $(\xi,\eta)=(2\pi-2\gamma,0)$ lies apart from singularities of the coordinate system which creates a local problem for numerical treatment, however, this singularity is repulsive and produces less an effect on the spacial structure of the wave function.

Equation (12) is written in a form that suggests treating the variables R and (ξ,η) separately. Indeed, following the hyperspherical method [20–22] in solving this equation we are going to exploit the idea of adiabatic separability between R and (ξ,η). Among several currently used technologies of implementing this idea in practical calculations the one proposed in [6] has proven to be the most efficient. Following [6] we seek the solutions to Eq. (12) in the form of the slow/smooth variable discretization (SVD) expansion

$$\Psi(R,\xi,\eta)=\frac{1}{R^{3/2}}\sum_{i=1}^{N_{\rm DVR}}\sum_{\nu}c_{i\nu}\pi_i(R)\Phi_\nu(\xi,\eta;R_i). \quad (17)$$

Here the radial part is represented by a finite set of interrelated points R_i and basis functions $\pi_i(R)$, $i=1,\ldots,N_{\rm DVR}$, whose most essential property is

$$\int \pi_i(R)H_{\rm ad}(R)\pi_j(R)dR=\delta_{ij}H_{\rm ad}(R_i), \quad (18)$$

where the integration goes over the interval of R where expansion (17) applies. The particular choice of this set depends on the asymptotic boundary condition and for the present case will be specified in the next section. The angular part in Eq. (17) is represented by the solutions of the HSA eigenvalue problem

$$[H_{\rm ad}(R)-U_\nu(R)]\Phi_\nu(\xi,\eta;R)=0. \quad (19)$$

This equation subject to the regularity boundary conditions has only a discrete spectrum of solutions which depend on R as a parameter. The eigenvalues $U_\nu(R)$ converted to

$$W_\nu(R)=\frac{U_\nu(R)+15/8}{R^2} \quad (20)$$

and the eigenfunctions $\Phi_\nu(\xi,\eta;R)$ numbered by $\nu=1,2,\ldots$ in order of increasing $U_\nu(R)$ are called the HSA potentials and channel functions, respectively. For any R, the HSA channel functions form a complete orthogonal basis on hypersphere. We normalize it by

$$\langle\Phi_\nu|\Phi_\mu\rangle=\delta_{\nu\mu}, \quad (21)$$

where the notation $\langle\cdots\rangle$ means

$$\langle F\rangle\equiv\int_{2\gamma}^{2\pi-2\gamma}d\xi\int_{-2\gamma}^{2\gamma}d\eta(\cos\eta-\cos\xi)\times F(\xi,\eta) \quad (22)$$

for an arbitrary $F(\xi,\eta)$. Substituting expansion (17) into Eq. (12) one can obtain a set of algebraic equations defining the coefficients $c_{i\nu}$. This will be done in the next section, while of the tasks here it remains to describe our method of solving the HSA eigenvalue problem (19).

The method is based on the recently found symmetry of the three-body Coulomb problem [4] which affords approximate separation of the variables ξ and η in Eq. (19). The idea is to substitute Eq. (19) by an auxiliary separable problem which is much easier to solve and whose solutions will provide a basis for subsequent variational solution of Eq. (19). To implement this approach, first of all it should be noted that the grand angular momentum operator (14), which plays a role of the kinetic energy in Eq. (19), is separable in the HSE coordinates (ξ,η). A general functional structure of the potential energy which is separable in these coordinates simultaneously with Λ_0^2 is

$$C^{(\rm s)}(\xi,\eta)=\frac{a(\xi)+b(\eta)}{\cos\eta-\cos\xi}, \quad (23)$$

where $a(\xi)$ and $b(\eta)$ are arbitrary functions. We split the effective charge (15) into two parts,

$$C(\xi,\eta)=C^{(\rm s)}(\xi,\eta)+C^{(\rm r)}(\xi,\eta), \quad (24)$$

where $C^{(\rm s)}(\xi,\eta)$ is given by Eq. (23) and thus is separable, and $C^{(\rm r)}(\xi,\eta)$ is the residue. Let us proceed leaving the functions $a(\xi)$ and $b(\eta)$ undefined for the moment. We introduce separable approximations to the HSA Hamiltonian (13),

$$H_{\rm ad}^{(\rm s)}(R)=\frac{1}{2}\Lambda_0^2+RC^{(\rm s)}(\xi,\eta), \quad (25)$$

and to the HSA eigenvalue problem (19),

$$[H_{\rm ad}^{(\rm s)}(R)-U_{\nu_{\rm s}}^{(\rm s)}(R)]\Phi_{\nu_{\rm s}}^{(\rm s)}(\xi,\eta;R)=0. \quad (26)$$

Seeking the solutions to this equation in the form

$$\Phi_{\nu_{\rm s}}^{(\rm s)}(\xi,\eta;R)=f_{\nu_{\rm s}}(\xi;R)g_{\nu_{\rm s}}(\eta;R), \quad (27)$$

for the functions $f_{\nu_{\rm s}}(\xi;R)$ and $g_{\nu_{\rm s}}(\eta;R)$ one obtains

$$\left[8\frac{d}{d\xi}(\cos2\gamma-\cos\xi)\frac{d}{d\xi}-Ra(\xi)+U_{\nu_{\rm s}}^{(\rm s)}(R)(\cos2\gamma-\cos\xi)-A_{\nu_{\rm s}}(R)\right]f_{\nu_{\rm s}}(\xi;R)=0, \quad (28a)$$

$$\left[8\frac{d}{d\eta}(\cos\eta-\cos2\gamma)\frac{d}{d\eta}-Rb(\eta)+U_{\nu_{\rm s}}^{(\rm s)}(R)(\cos\eta-\cos2\gamma)+A_{\nu_{\rm s}}(R)\right]g_{\nu_{\rm s}}(\eta;R)=0, \quad (28b)$$

where $A_{\nu_s}(R)$ is the separation constant. Thus each solution (27) can be characterized by a pair of eigenvalues $U^{(s)}_{\nu_s}(R)$ and $A_{\nu_s}(R)$ giving the integrals of motion of the separable problem (26) or, alternatively, by a pair of the hyperspherical elliptic quantum numbers n_ξ and n_η giving the numbers of zeros of the solutions to Eqs. (28a) and (28b), respectively. This specifies the index ν_s labeling the solutions (27) as

$$\nu_s=(n_\xi,n_\eta), \quad n_\xi,n_\eta=0,1,\ldots. \tag{29}$$

Functions (27) provide a basis for expanding the HSA channel functions,

$$\Phi_\nu(\xi,\eta;R)=\sum_{\nu_s} v_{\nu_s\nu}\Phi^{(s)}_{\nu_s}(\xi,\eta;R). \tag{30}$$

Substituting this expansion into Eq. (19) one obtains an algebraic eigenvalue problem defining the HSA potentials $U_\nu(R)$ and the coefficients $v_{\nu_s\nu}$:

$$\sum_{\mu_s}\{RC^{(r)}_{\nu_s\mu_s}+[U^{(s)}_{\nu_s}(R)-U_\nu(R)]\delta_{\nu_s\mu_s}\}v_{\mu_s\nu}=0, \tag{31}$$

where

$$C^{(r)}_{\nu_s\mu_s}=\langle\Phi^{(s)}_{\nu_s}|C^{(r)}|\Phi^{(s)}_{\mu_s}\rangle \tag{32}$$

and it is assumed that the separable basis (27) is normalized by the same condition (21).

Now we have to define the potential functions $a(\xi)$ and $b(\eta)$. The evident goal in choosing them is to minimize the term $C^{(r)}_{\nu_s\mu_s}$ in Eq. (31), i.e., to minimize the role of the nonseparable part of the potential (24). The best separable approximation would be obtained by defining these functions self-consistently [5]. However our experience shows that it is much more convenient in practice to use the asymptotically adapted potentials defined by [5]

$$a(\xi)=(\cos\eta-\cos\xi)C(\xi,\eta)\big|_{\eta=2\gamma}, \tag{33a}$$

$$b(\eta)=[(\cos\eta-\cos\xi)C(\xi,\eta)-a(\xi)]\big|_{\xi=2\gamma}. \tag{33b}$$

This causes no a substantial loss in the quality of separability. Indeed, as was already mentioned above, except at small R the HSA channel functions $\Phi_\nu(\xi,\eta;R)$ are localized near two attractive Coulomb singularities at $(\xi,\eta)=(2\gamma,\pm2\gamma)$, therefore for good separability function (23) must approximate the effective charge $C(\xi,\eta)$ most importantly in the vicinity of these points. It can be shown that for $a(\xi)$ and $b(\eta)$ defined by Eqs. (33)

$$(\cos\eta-\cos\xi)C(\xi,\eta)\big|_{(\xi,\eta)\to(2\gamma,\pm2\gamma)}=a(\xi)+b(\eta)+\mathcal{O}[(\xi-2\gamma)(\eta\mp2\gamma)]. \tag{34}$$

Thus functions (33) not only correctly reproduce the constant terms in the expansion of the left hand side in Eq. (34) which define the two-body Coulomb spectrum of the asymptotic values of the HSA potentials (20) at $R\to\infty$, but also the linear terms which define the Stark splitting. The relationship between the HSA eigenvalue problem (19) and the separable approximation to it (26) can be summarized as follows: The separability becomes exact in each of the limits $R\to0$ and $R\to\infty$ and holds approximately in between. Besides, the separability depends on M and, as will be shown in Sec. III A, becomes exact in the molecular limit $M\to\infty$. Thus HSA potentials and channel functions can be approximately classified by the HSE quantum numbers (29), and this classification applies universally throughout the whole range of R and to all the systems.

Let us comment on the accuracy of this method of solving Eq. (19). It is relatively easy to solve Eqs. (28) with the accuracy of the eigenvalues $U^{(s)}_{\nu_s}(R)$ and $A_{\nu_s}(R)$ approaching the machine precision. Thus obtained separable basis (27) is in one-to-one correspondence with the solutions of Eq. (19), that is for each HSA channel function there is a single dominant term in expansion (30) whose contribution to the norm approaches 1 at $R\to0$ and $R\to\infty$ and is typically of the order 0.9 in between, excluding the localized regions of the avoided crossings of the HSA potentials (20). So the variational error caused by inevitable truncating expansion (30) to a finite number of terms is not essential and can be easily reduced. In our calculations the number of separable basis functions usually exceeds the desired number of HSA channel functions by a factor 2–3. It should be noted that for symmetric systems and states of ''singlet'' symmetry of interest here only terms with even n_η should be included in expansion (30). The principal source of errors in the present numerical scheme is the repulsive Coulomb singularity arising from the second term in Eq. (15). This singularity prevents achieving high precision in calculating matrix elements (32) which limits the final accuracy of the HSA potentials by a relative error $\sim10^{-8}$.

We finish discussing the HSE-SVD representation by the following remark. Taking into account good separability of Eq. (19) one could skip the step of solving Eq. (31) and switch in the SVD expansion (17) from HSA to separable angular basis,

$$\Psi(R,\xi,\eta)=\frac{1}{R^{3/2}}\sum_{i=1}^{N_{\rm DVR}}\sum_{\nu_s}\tilde{c}_{i\nu_s}\pi_i(R)f_{\nu_s}(\xi;R_i)g_{\nu_s}(\eta;R_i). \tag{35}$$

This approach would open the possibility to perform a selective choice of the separable basis functions to be included in expansion (35) depending on their HSE quantum numbers (29), which may greatly simplify treating states belonging to higher HSA channels. However for the present purposes it is preferable to stick to Eq. (17).

B. Siegert pseudostate (SPS) eigenvalue problem

The HSE-SVD representation summarized above provides a framework which enables one to calculate different properties of and processes in three-body Coulomb systems. In this section we show how using this representation in combination with the SPS method introduced in [2] and more fully developed in [3] one can calculate resonances. To this end we have to complete the previous formulation by specifying those its elements which depend on the problem and have been left undefined above.

First, we discuss the asymptotic boundary condition. Following the approach pioneered by Siegert [1] we shall seek

resonances among the solutions to the Schrödinger equation (12) which contain only outgoing waves at $R\to\infty$. Taking into account the requirement of regularity of the wave function Ψ, such solutions may exist only for a discrete set of generally complex energies E, thus we are dealing with an eigenvalue problem. The solutions to this problem are called Siegert states. For practical purposes it is convenient to introduce Siegert *pseudostates* defined as solutions to Eq. (12) satisfying the outgoing wave boundary condition imposed at a *finite* distance from the origin [2],

$$\left(\frac{\partial}{\partial R}-ik\right)R^{5/2}\Psi(R,\xi,\eta)\bigg|_{R=R_m}=0. \tag{36}$$

Here the momentum k is related with the energy E that appears in Eq. (12) by

$$E=E_0+k^2/2, \tag{37}$$

where

$$E_0=-\mu/2 \tag{38}$$

is the ground state energy for each of the pairs 1–3 and 2–3 giving the boundary of the continuum for the present problem, and

$$\mu=\frac{M}{1+M} \tag{39}$$

is the reduced mass of the particles 1 (or 2) and 3. Equation (36) restricts the region of configuration space to be considered in calculations by the interior of the hypersphere of radius R_m, which renders the SPS method practical. However simultaneously this makes the results dependent on the cutoff radius R_m, and it should be understood that for obtaining physically meaningful results one must analyze convergence as R_m increases. As was demonstrated in [3], the SPS eigenvalues corresponding to individually observable states of the system, which includes bound, weakly antibound, and narrow resonance states, rapidly stabilize as R_m grows; the others never do. Thus resonances can be calculated by solving the SPS eigenvalue problem, Eqs. (12) and (36), and looking for such solutions that become independent of R_m for sufficiently large values of this parameter. Other computational possibilities in scattering theory opened by the SPS formulation are discussed in [2,3].

Next, we define the radial basis in the SVD expansion (17). In order to satisfy Eq. (18) it is convenient to use a discrete variable representation (DVR) basis [23] constructed of suitable orthogonal polynomials [6]. The polynomials should be chosen taking into account that the wave function (17) must satisfy the regularity boundary condition at $R=0$ and the outgoing wave boundary condition (36) at $R=R_m$. Restricting ourselves to classical orthogonal polynomials, these conditions define the radial basis uniquely. For numerical treatment it is convenient to introduced a new variable x instead of R,

$$x=2R/R_m-1, \quad R=\tfrac{1}{2}R_m(1+x), \tag{40}$$

which transforms the interval $0\leqslant R\leqslant R_m$ into $-1\leqslant x\leqslant 1$. Then the radial basis is defined by

$$\pi_i(x)=(1+x)^{3/2}\sum_{n=1}^{N_{\rm DVR}}\sqrt{\omega_i}\,\widetilde{P}_{n-1}^{(0,3)}(x_i)\widetilde{P}_{n-1}^{(0,3)}(x). \tag{41}$$

Here $\widetilde{P}_n^{(0,3)}(x)$, $n=0,1,\ldots,$ are Jacobi polynomials orthogonal on the interval $x\in[-1,1]$ with the weight $(1+x)^3$, where the tilde means that the polynomials are normalized, so that

$$\int_{-1}^{1}\pi_i(x)\,\pi_j(x)dx=\delta_{ij}, \tag{42}$$

and x_i, ω_i, $i=1,2,\ldots,N_{\rm DVR}$, are abscissas and weights of the corresponding $N_{\rm DVR}$-point Gauss-Jacobi quadrature. This basis satisfies Eq. (18), where the integration over $R\in[0,R_m]$ should be replaced by the integration over $x\in[-1,1]$. The points R_i in Eqs. (17) and (18) are defined by x_i via Eqs. (40).

Substituting expansion (17) into Eq. (12) and using Eqs. (18), (19), (36), and (42) we obtain the HSE-SVD representation of the SPS eigenvalue problem,

$$[(\mathbf{K}+\mathbf{L}+\mathbf{U}-E_0\boldsymbol{\rho})-ikR_m\mathbf{L}-\tfrac{1}{2}k^2\boldsymbol{\rho}]c=0. \tag{43}$$

Here c is the vector of coefficients in Eq. (17), and the boldface characters denote the SVD matrices defined by their matrix elements:

$$\mathbf{K}_{i\nu,j\mu}=K_{ij}O_{i\nu,j\mu} \quad \text{—radial kinetic energy,} \tag{44a}$$

$$\boldsymbol{\rho}_{i\nu,j\mu}=\rho_{ij}O_{i\nu,j\mu} \quad \text{—radial weight,} \tag{44b}$$

$$\mathbf{L}_{i\nu,j\mu}=L_{ij}O_{i\nu,j\mu} \quad \text{—Bloch operator,} \tag{44c}$$

$$\mathbf{U}_{i\nu,j\mu}=U_\nu(R_i)\,\delta_{i\nu,j\mu} \quad \text{—HSA potential energy,} \tag{44d}$$

where

$$K_{ij}=\frac{1}{2}\int_{-1}^{1}\frac{d\pi_i(x)}{dx}(1+x)^2\frac{d\pi_j(x)}{dx}dx+\frac{15}{8}\delta_{ij}, \tag{45a}$$

$$\rho_{ij}=\frac{1}{4}R_m^2\int_{-1}^{1}\pi_i(x)(1+x)^2\pi_j(x)dx, \tag{45b}$$

$$L_{ij}=\pi_i(1)\,\pi_j(1) \tag{45c}$$

are the DVR matrices, and

$$O_{i\nu,j\mu}=\langle\Phi_\nu(\xi,\eta;R_i)|\Phi_\mu(\xi,\eta;R_j)\rangle \tag{46}$$

is the overlap matrix. The DVR matrices (45) can be calculated analytically, see Appendix C in [3]. They have the dimension $N_{\rm DVR}$. The HSA potentials (44d) and the overlap matrix (46) can be obtained by solving the HSA eigenvalue problem (19). Retaining the $N_{\rm ch}$ lowest HSA channels in the SVD expansion (17), the SVD matrices (44) will have the dimension $N_{\rm SVD}=N_{\rm DVR}N_{\rm ch}$. Having thus defined all the matrices in Eq. (43), it remains to solve the equation. Notice that this is a quadratic eigenvalue problem with respect to k.

The desired resonance eigenvalue can be found iteratively which, however, requires to know a good initial guess. Alternatively, Eq. (43) can be linearized by reducing to the form

$$\begin{pmatrix} \mathbf{0} & \mathbf{I} \\ -2\boldsymbol{\rho}^{-1}(\mathbf{K}+\mathbf{L}+\mathbf{U})+2E_0 & 2\boldsymbol{\rho}^{-1}R_m\mathbf{L} \end{pmatrix} \begin{pmatrix} c \\ ikc \end{pmatrix} = ik \begin{pmatrix} c \\ ikc \end{pmatrix}, \tag{47}$$

where $\mathbf{0}$ and $\mathbf{I}$ are zero and unit matrices of the dimension N_{SVD}. This is a linear eigenvalue problem with respect to k of the doubled dimension $2N_{\mathrm{SVD}}$ and it can be solved by standard routines.

C. Results

Before discussing results, let us summarize the basic steps of the present numerical procedure. For a given value of the mass ratio M one has:

(i) To fix the parameters R_m and N_{DVR} of the SVD expansion (17) and to solve the HSA eigenvalue problem (19) for the N_{DVR} values of hyperradius $R=R_i$ retaining the N_{ch} lowest solutions.

(ii) To calculate the overlap matrix (46) and to construct the matrices in Eq. (43).

(iii) To solve the SPS eigenvalue problem in either of the forms Eq. (43) or Eq. (47).

(iv) To repeat the previous steps for increased values of R_m, N_{DVR}, and N_{ch} until convergence of the eigenvalue representing the desired resonance state with respect to each of these parameters is achieved.

This procedure yields the resonance position $\mathcal{E}$ and width Γ for the given M. Repeating it for different values of M one obtains the functions $\mathcal{E}(M)$ and $\Gamma(M)$ which are in the focus of the present study. In this section we report the numerical results.

1. Hyperspherical adiabatic potentials

Figure 1 shows two lowest HSA potentials defined by Eqs. (19) and (20) calculated for three representative systems ranging from the atomic ($M\to 0$) to the molecular ($M\to\infty$) limit of the mass-ratio spectrum, see Table I. The M-dependent factors multiplying $W_\nu(R)$ and R are introduced in order to bring systems corresponding to vastly different values of M to a common scale in this figure. These factors result from the following consideration. In the system of units we use here (m.a.u.) a characteristic energy is given by the reduced mass μ of the particles 1 (or 2) and 3, see Eq. (39). Dividing $W_\nu(R)$ by μ makes the curves shown in Fig. 1 to converge to the same ''hydrogenic'' thresholds at $R\to\infty$, namely, to -0.5 for $\nu=1$ and to -0.125 for $\nu=2$, independently of M. We shall use this reduced energy scale for presenting all the results in this section. A characteristic interparticle distance is $1/\mu$ and, as follows from Eqs. (2) and (7), a characteristic value of the hyperradius R then is $\sqrt{M}/\mu$. Dividing R by this factor leads to a good coincidence between the positions of the minimum of the lowest curve for all values of M. The additional factor $\sqrt{2}$ is introduced to make the abscissa in Fig. 1 equal to the distance between the heavy particles 1 and 2 in the molecular limit $M\to\infty$, see Sec. III A. The potential curves shown in Fig. 1 provide the minimum theoretical input needed for discussing the resonance state of interest here. This state can be defined as the lowest Feshbach resonance supported by the upper ($\nu=2$) potential curve, while the lower ($\nu=1$) curve represents the only decay channel. The $\nu=1$ and $\nu=2$ HSA channels can be classified by the HSE quantum numbers (n_ξ,n_η) of the dominant separable component in expansion (30) as (0,0) and (0,2), respectively. So the resonance state of interest here can be identified by the triple $(n_\xi,n_\eta,\nu)=(0,2,0)$, where ν is the vibrational quantum number defining the motion in R.

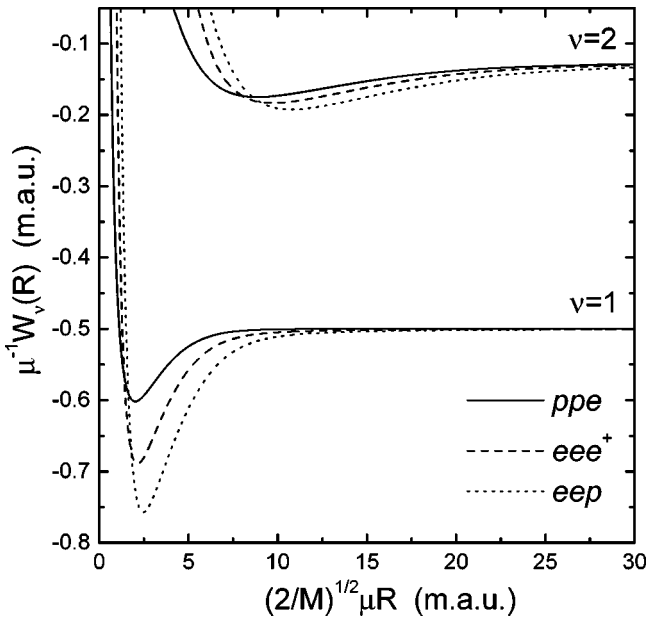

FIG. 1. Two lowest hyperspherical adiabatic potentials $W_\nu(R)$ defined by Eqs. (19) and (20) as functions of the hyperradius R defined by Eq. (7) for three representative systems ranging from the atomic ($M=0$) to the molecular ($M=\infty$) limit of the mass-ratio M, see Table I. The upper potential supports the resonance state of interest here, while the lower one represents the only decay channel. μ is the reduced mass for each of the pairs which can form a bound state, see Eq. (39) . Here and in all the following figures and tables in this paper, m.a.u. stands for modified atomic units defined in the beginning of Sec. II.

2. Siegert pseudostate eigenvalues

Figure 2 gives an example of the distribution of the SPS eigenvalues in complex energy plain calculated for the eee^+ system with some particular values of the parameters R_m, N_{DVR}, and N_{ch}. The eigenvalues were obtained by solving Eq. (47) and converting from the momentum k to the energy E domain using Eq. (37). Some general features of this distribution common to all systems studied can be summarized as follows. (i) For the lowest HSA channel, there is a finite number of real eigenvalues lying on the left of the channel threshold -0.5 (notice the reduced energy scale in the figure) which represent bound (exponentially decaying) or antibound (exponentially growing without an admixture of the decaying solution) states supported by this channel. In the case shown in Fig. 2, there is one bound and one antibound

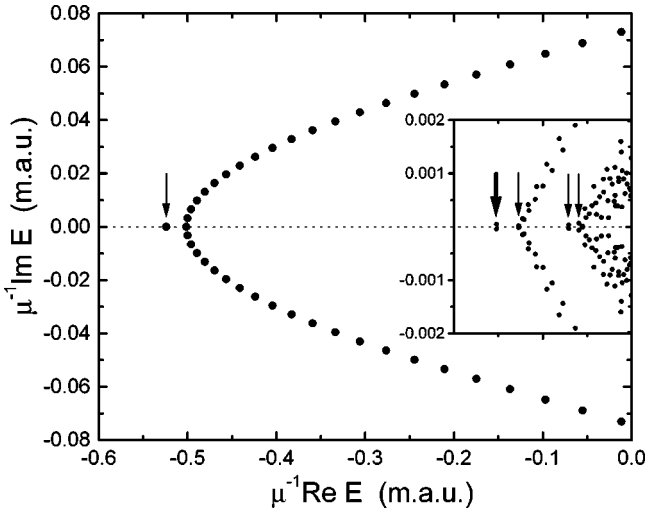

FIG. 2. The distribution of the Siegert pseudostate energy eigenvalues defined by Eqs. (37) and (43) [or (47)] for the eee^+ system ($M=1$) calculated with the parameters $R_m=100$, $N_{\mathrm{DVR}}=60$, and $N_{\mathrm{ch}}=40$. All the eigenvalues shown are converged with respect to N_{DVR} and N_{ch}. The arrows indicate the eigenvalues that also converge as R_m grows. The bold arrow indicates the resonance state of interest here. Notice that the vertical scale in the box is extended with respect to that in the rest of the figure by the factor of 20.

eigenvalue lying on the top of each other indicated by the leftmost arrow. Besides these real eigenvalues, there is a parabola-like branch formed by complex eigenvalues lying on the right of the channel threshold which represent the discretized continuum of the lowest channel. (ii) This structure repeats itself for higher HSA channels with one difference: the eigenvalues lying on the left of the channel threshold acquire an imaginary part and represent resonance states supported by the channel. Because of the Coulomb degeneracy, there are n HSA channels converging to the nth hydrogenic threshold $-0.5/n^2$ at $R\to\infty$ and, consequently, there are n parabola-like branches representing discretized continua, one for each of the channels. In Fig. 2 one can clearly distinguish the described structure around the three lowest thresholds $n=1$, 2, and 3; to resolve higher thresholds the cutoff radius R_m must be increased.

Now we discuss how this distribution depends on the parameters R_m, N_{DVR}, and N_{ch}. The latter two parameters define the size of the basis in the SVD expansion (17). All the SPS eigenvalues rather rapidly converge as N_{DVR} and N_{ch} increase, and the farther on the left they lie in Fig. 2 the faster they converge. Thus all the eigenvalues shown in the figure are converged with respect to N_{DVR} and N_{ch}. The dependence of the eigenvalues on the cutoff radius R_m is quite different. In accordance with the results of [3], only the bound and resonance state eigenvalues converge as R_m grows; all the others never do, becoming instead more and more densely distributed along the continuum branches. The converging eigenvalues are indicated by arrows in Fig. 2. The lowest resonance lying on the left of the second hydrogenic threshold -0.125 and indicated by the bold arrow is the one we are interested in here. In the following, only this resonance state will be discussed.

3. Convergence

Tables II–VI demonstrate convergence of the resonance parameters $\mathcal{E}$ and Γ calculated for several representative realistic systems. The corresponding values of the mass-ratio M used in the calculations are given in Table I. In all the cases, the resonance position $\mathcal{E}$ converges rather easily within at least six significant digits. This level of accuracy agrees with that of our earlier calculations of bound and resonance states in various three-body Coulomb systems. As was mentioned above, in the present numerical scheme it is limited by the accuracy of calculating matrix elements (32). As can be seen from the tables, the accuracy of calculating the resonance width Γ rapidly deteriorates as M grows, and this is understandable. In the present method $\mathcal{E}$ and Γ are obtained via Eq. (1) from the real and imaginary parts of the same complex number giving the SPS energy eigenvalue. So the ratio $\Gamma/\mathcal{E}$ is limited from below by round-off errors which are not less than 10^{-12} using the double precision arithmetic. As M grows, Γ rapidly decreases while $\mathcal{E}$ stays almost constant, and the ratio $\Gamma/\mathcal{E}$ reaches this limit already for $M\approx 30$. This sets an upper boundary on the values of M which can be treated by the present method. Accordingly, in the following we restrict ourselves to reporting results only for the interval $0\leqslant M\leqslant 30$. It should be noted that this interval includes most of the realistic systems listed in Table I. Besides demonstrating convergence, Tables II–VI present the converged results which are the best reported estimates of the resonance parameters for the considered systems as can be seen from the comparison with other calculations, when available.

4. Final results

Our final results for the functions $\mathcal{E}(M)$ and $\Gamma(M)$ are presented in Table VII and shown by solid circles and squares in Fig. 3. They were calculated with the parameters R_m, N_{DVR}, and N_{ch} varying with M, as dictated by the tests of convergence discussed above. The resonance position $\mathcal{E}(M)$ is a featureless function. Multiplied by μ^{-1}, it is bounded by the second hydrogenic threshold -0.125 from above and by the minimum of the $\nu=2$ curve in Fig. 1 taken as a function of M from below. The arrow in Fig. 3(a) indicates the position of this minimum in the limit $M\to\infty$; the corresponding numerical value is given in the last entry of Table VII. As M grows, $\mathcal{E}(M)$ monotonically approaches this value from above. Such behavior of $\mathcal{E}(M)$ could be expected *a priori* looking at Fig. 1, and the heavy calculations reported here merely provide accurate numbers. The situation with the resonance width $\Gamma(M)$ is quite different. The decay of the resonance occurs via nonadiabatic coupling between HSA channels which corresponds to energy exchange between different degrees of freedom in the system. As M grows, two of the particles become much heavier than the third one, and the energy exchange becomes less efficient, so that $\Gamma(M)$ must decrease vanishing in the limit $M\to\infty$, as is indicated in the last entry of Table VII. However along with this expected decreasing the function $\Gamma(M)$ exhibits rather unexpected oscillations. It has five distinct minima in the interval $0\leqslant M\leqslant 30$ at $M\approx 1.54$, 5.77, 11.6, 19.1, and 28.0 where it becomes vanishingly small. For locating their positions we have performed additional calculations whose results are not included in Table VII but are shown in Fig. 3(b). As can be seen from the figure, the values of $\Gamma(M)$ at adjacent minima and maxima differ by several orders of magnitude, so the oscillations are very pronounced. Discovering these oscillations is the principal result of the calcula-

TABLE II. Convergence of the present calculations of the lowest $^1S^e$ resonance state in eep with respect to the cutoff radius R_m and the numbers of the radial basis functions N_{DVR} and the HSA channel functions N_{ch} in the SVD expansion (17). The resonance position $\mathcal{E}$ and width Γ were obtained from the corresponding SPS energy eigenvalue via Eq. (1) and are given in m.a.u. The numbers in parentheses give the uncertainty in the last digit quoted. The converged values of the resonance parameters are $\mathcal{E}=-0.148695(1)$ a.u. and $\Gamma=0.1731(1)\times10^{-2}$ a.u., in agreement with Ref. [2]. We are not aware of any other calculations of this resonance state for a finite value of the proton mass.

		$-\mu^{-1}\mathcal{E}$		
R_m	N_{DVR}/N_{ch}	10	20	30
40	40	0.148 774 7	0.148 775 3	0.148 7756
—	50	0.148 774 7	0.148 775 3	0.148 7755
50	40	0.148 774 6	0.148 775 2	0.148 7754
—	50	0.148 774 7	0.148 775 2	0.148 7754
—	60	0.148 774 7	0.148 775 2	0.148 7754
60	60	0.148 775 0	0.148 775 6	0.148 7758
70	60	0.148 774 8	0.148 775 4	0.148 7756
Converged				0.148 775(1)
		$10^2\times\mu^{-1}\Gamma$		
R_m	N_{DVR}/N_{ch}	10	20	30
40	40	0.173 21	0.173 17	0.173 17
—	50	0.173 21	0.173 17	0.173 17
50	40	0.173 20	0.173 18	0.173 19
—	50	0.173 22	0.173 19	0.173 19
—	60	0.173 22	0.173 18	0.173 19
60	60	0.173 19	0.173 17	0.173 18
70	60	0.173 18	0.173 13	0.173 14
Converged				0.1732(1)

TABLE III. The same as in Table II, but for eee^+. The converged values of the resonance parameters are $\mathcal{E}=-0.076\,0304(1)$ a.u. and $\Gamma=0.4304(1)\times10^{-4}$ a.u. The complex rotation results for this resonance state are $\mathcal{E}=-0.07\,60304$ a.u. and $\Gamma=0.43\times10^{-4}$ a.u. [24].

				$-\mu^{-1}\mathcal{E}$		
R_m	N_{DVR}/N_{ch}	10	20	30	40	50
100	40	0.152 0581	0.152 0605	0.152 0608	0.152 0608	0.152 0609
—	50	0.152 0582	0.152 0605	0.152 0608	0.152 0608	0.152 0609
—	60	0.152 0581	0.152 0605	0.152 0608	0.152 0608	0.152 0609
150	50	0.152 0586	0.152 0608	0.152 0611	0.152 0611	0.152 0611
—	60	0.152 0582	0.152 0605	0.152 0608	0.152 0608	0.152 0609
—	70	0.152 0582	0.152 0605	0.152 0608	0.152 0608	
Converged						0.152 061(1)
				$10^4\times\mu^{-1}\Gamma$		
R_m	N_{DVR}/N_{ch}	10	20	30	40	50
100	40	0.860 87	0.860 62	0.860 71	0.860 58	0.860 60
—	50	0.859 01	0.860 76	0.860 67	0.860 57	0.860 59
—	60	0.859 95	0.860 64	0.860 66	0.860 60	0.860 59
150	50	0.861 25	0.862 73	0.862 31	0.862 06	0.861 67
—	60	0.858 85	0.860 72	0.860 80	0.860 71	0.860 73
—	70	0.859 12	0.860 76	0.860 79	0.860 75	
Converged						0.8607(1)

TABLE IV. The same as in Table II, but for $pp\mu$. The converged values of the resonance parameters are $\mathcal{E}=-0.146\,404(1)\,\mu$ a.u. and $\Gamma=0.304(1)\times10^{-6}\,\mu$ a.u.

			$-\mu^{-1}\mathcal{E}$	
R_m	$N_{\rm DVR}/N_{\rm ch}$	10	20	30
70	40	0.162 8874	0.162 8903	0.162 8909
—	50	0.162 8874	0.162 8903	0.162 8909
—	60	0.162 8874	0.162 8903	0.162 8909
90	50	0.162 8874	0.162 8903	0.162 8909
—	60	0.162 8874	0.162 8903	0.162 8909
—	70	0.162 8874	0.162 8903	0.162 8909
130	80	0.162 8874	0.162 8903	0.162 8909
Converged				0.162891(1)
			$10^6\times\mu^{-1}\Gamma$	
R_m	$N_{\rm DVR}/N_{\rm ch}$	10	20	30
70	40	0.3391	0.3388	0.3383
—	50	0.3383	0.3387	0.3383
—	60	0.3373	0.3386	0.3382
90	50	0.3384	0.3383	0.3378
—	60	0.3364	0.3374	0.3369
—	70	0.3361	0.3378	0.3379
130	80	0.3365	0.3380	0.3378
Converged				0.338(1)

TABLE V. The same as in Table II, but for $dd\mu$. The converged values of the resonance parameters are $\mathcal{E}=-0.157\,099(1)\,\mu$ a.u. and $\Gamma=0.69(1)\times10^{-9}\,\mu$ a.u., in agreement with Ref. [2]. The variational result for the position of this resonance state is $\mathcal{E}=-0.15\,7\,099\mu$ a.u. [25].

			$-\mu^{-1}\mathcal{E}$	
R_m	$N_{\rm DVR}/N_{\rm ch}$	10	20	30
90	50	0.165 9466	0.165 9483	0.165 9487
—	60	0.165 9466	0.165 9483	0.165 9487
—	70	0.165 9466	0.165 9483	0.165 9487
110	60	0.165 9466	0.165 9483	0.165 9487
—	70	0.165 9466	0.165 9483	0.165 9487
—	80	0.165 9466	0.165 9483	0.165 9487
160	90	0.165 9466	0.165 9483	0.165 9487
Converged				0.165 949(1)
			$10^9\times\mu^{-1}\Gamma$	
R_m	$N_{\rm DVR}/N_{\rm ch}$	10	20	30
90	50	0.731	0.743	0.729
—	60	0.748	0.744	0.727
—	70	0.723	0.744	0.726
110	60	0.750	0.742	0.727
—	70	0.723	0.743	0.725
—	80	0.718	0.743	0.726
160	90	0.721	0.743	0.725
Converged				0.73(1)

TABLE VI. The same as in Table II, but for $tt\mu$. The converged values of the resonance parameters are $\mathcal{E}=-0.161\,370(1)\,\mu$ a.u. and $\Gamma=0.3(1)\times10^{-10}\,\mu$ a.u.

			$-\mu^{-1}\mathcal{E}$	
R_m	$N_{\rm DVR}/N_{\rm ch}$	10	20	30
90	60	0.167 4386	0.167 4396	0.167 4399
—	70	0.167 4386	0.167 4396	0.167 4399
110	70	0.167 4386	0.167 4396	0.167 4399
—	80	0.167 4386	0.167 4396	
160	90	0.167 4386	0.167 4396	0.167 4399
Converged				0.167440(1)
			$10^{10}\times\mu^{-1}\Gamma$	
R_m	$N_{\rm DVR}/N_{\rm ch}$	10	20	30
90	60	0.65	0.76	0.64
—	70	0.65	0.75	0.60
110	70	0.21	0.38	0.20
—	80	0.21	0.34	
160	90	0.21	0.39	0.19
Converged				0.3(1)

tional part of this work. The remaining part of the paper is devoted to clarifying the underlying physical mechanism.

III. PERTURBATION ANALYSIS OF A SIMPLIFIED MODEL

The oscillations of the resonance width $\Gamma(M)$ found numerically in the previous section certainly require some qualitative interpretation. As a step towards such an interpretation, we believe it will be useful to consider a simplified model obtained from Eq. (12) in the limit

$$M\to\infty. \tag{48}$$

As will be shown in this section, this model preserves all the major features of the dependence on M of the full-scale three-body Coulomb problem discussed above but, at the same time, it is more transparent and unambiguously points to the direction where an explanation of the oscillations should be sought.

A. Born-Oppenheimer model

Consider equations of Sec. II A in the limit (48). In the following, all the quantities obtained in this limit from their counterparts in Sec. II A and properly rescaled, if needed, will be denoted by the same notation with a bar. But we shall

TABLE VII. Present accurate results for the position $\mathcal{E}(M)$ and width $\Gamma(M)$ of the lowest $^1S^e$ resonance in a family of symmetric three-body Coulomb systems as functions of the mass-ratio M. The results (in m.a.u.) are rounded to six and three significant digits for $\mathcal{E}(M)$ and $\Gamma(M)$, respectively, independently of the actual accuracy. $a[b]=a\times10^b$.

M	$-\mu^{-1}\mathcal{E}(M)$	$\mu^{-1}\Gamma(M)$	M	$-\mu^{-1}\mathcal{E}(M)$	$\mu^{-1}\Gamma(M)$
0	0.148 776	0.173[−02]	16	0.165 530	0.619[−08]
1	0.152 061	0.861[−04]	17	0.165 776	0.228[−08]
2	0.155 143	0.168[−04]	18	0.166 004	0.437[−09]
3	0.157 221	0.319[−04]	19	0.166 215	0.286[−11]
4	0.158 756	0.118[−04]	20	0.166 412	0.140[−09]
5	0.159 953	0.131[−05]	21	0.166 596	0.329[−09]
6	0.160 915	0.531[−07]	22	0.166 768	0.366[−09]
7	0.161 709	0.573[−06]	23	0.166 930	0.319[−09]
8	0.162 380	0.586[−06]	24	0.167 083	0.231[−09]
9	0.162 956	0.302[−06]	25	0.167 227	0.111[−09]
10	0.163 458	0.867[−07]	26	0.167 363	0.539[−10]
11	0.163 901	0.766[−08]	27	0.167 493	0.110[−10]
12	0.164 295	0.201[−08]	28	0.167 616	0.162[−11]
13	0.164 650	0.118[−07]	29	0.167 733	0.595[−11]
14	0.164 970	0.151[−07]	30	0.167 846	0.787[−11]
15	0.165 262	0.115[−07]	∞	0.175049	0

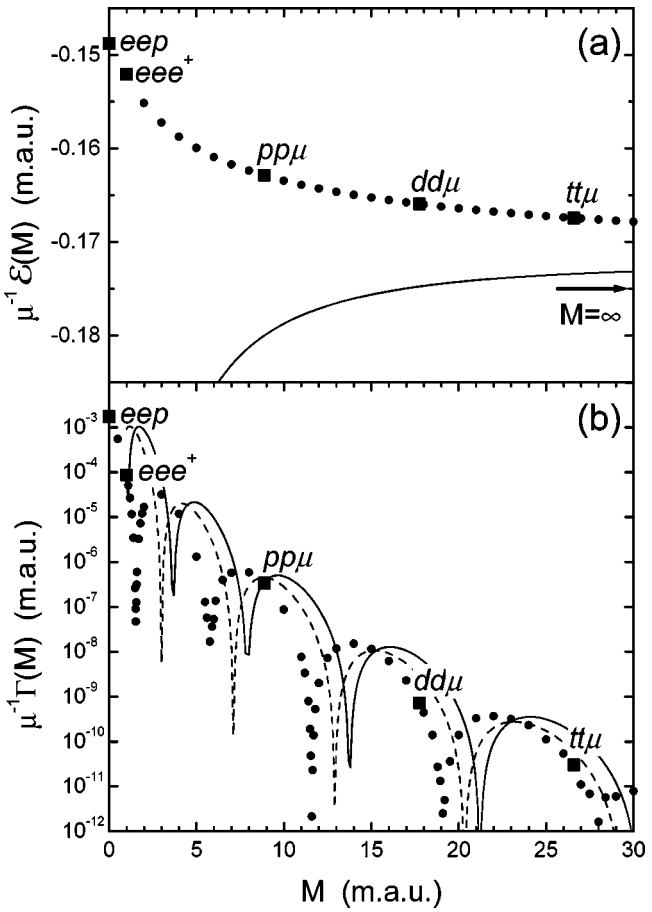

FIG. 3. Bold circles and squares: accurate results for the resonance position $\mathcal{E}(M)$ and width $\Gamma(M)$ calculated by the Siegert pseudostate method, the same as in Tables II–VII. Solid and dashed curves: the results obtained by perturbation analysis of the Born-Oppenheimer model. (a) The solid curve shows the results for $\mathcal{E}(M)$ obtained by solving Eqs. (68). The arrow indicates the value $\mathcal{E}(\infty)$ given in the last entry of Table VII. (b) The solid and dashed curves show the results for $\Gamma(M)$ calculated by Eqs. (71a) and (71b), respectively.

not put a bar over r_{ij} since the interparticle distances do not depend on the particles' masses. From Eq. (5) we have

$$\gamma|_{M\to\infty}=\sqrt{\frac{2}{M}}\to 0, \tag{49}$$

so the limit (48) can be also understood as $\gamma\to 0$. It is convenient to introduce new rescaled coordinates in configuration space,

$$\bar{R}\equiv \gamma R\big|_{M\to\infty}=r_{21}, \quad 0\leqslant\bar{R}\leqslant\infty, \tag{50}$$

$$\bar{\xi}\equiv \frac{\xi}{2\gamma}\bigg|_{M\to\infty}=\frac{r_{32}+r_{13}}{r_{21}}, \quad 1\leqslant\bar{\xi}\leqslant\infty, \tag{51}$$

$$\bar{\eta}\equiv \frac{\eta}{2\gamma}\bigg|_{M\to\infty}=\frac{r_{32}-r_{13}}{r_{21}}, \quad -1\leqslant\bar{\eta}\leqslant 1. \tag{52}$$

Here $\bar{R}$ is the distance between the heavy particles 1 and 2, and $(\bar{\xi},\bar{\eta})$ are plane elliptic coordinates defining the position of the light particle 3 in the coordinate system with foci at the particles 1 and 2. Note that the new coordinates $(\bar{R},\bar{\xi},\bar{\eta})$ do not depend on the mass-ratio M, in contrast to the coordinates (R,ξ,η) used above. The volume element (11) in these coordinates becomes

$$d\bar{V}\equiv\gamma^3 dV|_{M\to\infty}=\pi^2\bar{R}^5(\bar{\xi}^2-\bar{\eta}^2)d\bar{R}d\bar{\xi}d\bar{\eta}, \tag{53}$$

and the Schrödinger equation (12) takes the form

$$\left(-\frac{1}{M}\frac{\partial^2}{\partial\bar{R}^2}+\frac{\bar{H}_{\rm ad}(\bar{R})}{\bar{R}^2}-E\right)\bar{R}^{5/2}\Psi(\bar{R},\bar{\xi},\bar{\eta})=0. \tag{54}$$

Here

$$\bar{H}_{\rm ad}(\bar{R})\equiv\gamma^2 H_{\rm ad}(R)|_{M\to\infty}=\tfrac{1}{2}\bar{\Lambda}_0^2+\bar{R}\bar{C}(\bar{\xi},\bar{\eta}), \tag{55}$$

$$\bar{\Lambda}_0^2\equiv\gamma^2\Lambda_0^2|_{M\to\infty}=\frac{-4}{\bar{\xi}^2-\bar{\eta}^2}\left[\frac{\partial}{\partial\bar{\xi}}(\bar{\xi}^2-1)\frac{\partial}{\partial\bar{\xi}}+\frac{\partial}{\partial\bar{\eta}}(1-\bar{\eta}^2)\frac{\partial}{\partial\bar{\eta}}\right], \tag{56}$$

and

$$\bar{C}(\bar{\xi},\bar{\eta})\equiv\gamma C(\xi,\eta)|_{M\to\infty}=\frac{-4\bar{\xi}}{\bar{\xi}^2-\bar{\eta}^2}+1=\frac{\bar{a}(\bar{\xi})+\bar{b}(\bar{\eta})}{\bar{\xi}^2-\bar{\eta}^2}, \tag{57}$$

where

$$\bar{a}(\bar{\xi})\equiv\frac{a(\xi)}{2\gamma}\bigg|_{M\to\infty}=-1-4\bar{\xi}+\bar{\xi}^2, \tag{58a}$$

$$\bar{b}(\bar{\eta})\equiv\frac{b(\eta)}{2\gamma}\bigg|_{M\to\infty}=1-\bar{\eta}^2. \tag{58b}$$

In the operator (56) one can easily recognize the three-dimensional Laplacian multiplied by $-\bar{R}^2$ expressed in terms of the coordinates $(\bar{\xi},\bar{\eta})$, so $\bar{\Lambda}_0^2/(2\bar{R}^2)$ is the kinetic energy of the light particle 3. It should be noted that the azimuthal degree of freedom corresponding to the rotation of this particle about the axis joining the particles 1 and 2 is absent for the present case $L=0$, which explains the absence of the azimuthal term in Eq. (56). Function (57) is the potential energy of the system (16) multiplied by $\bar{R}$. Thus the second term in Eq. (54) gives the total energy of the light particle 3 moving in the potential field created by the two heavy particles 1 and 2 clamped in space at the distance $\bar{R}$ from each other plus the potential energy of interaction between them. This term does not depend on M. The first term in Eq. (54) is the kinetic energy of the relative motion of the heavy particles 1 and 2 where, again, the centrifugal energy corresponding to the rotation of the interparticle axis 1–2 is absent for the present case $L=0$. This term is inversely proportional to the reduced mass $M/2$ of the heavy particles and this is where all the dependence of Eq. (54) on M left in the limit (48) is concentrated.

For evident reasons, the system described by Eq. (54) will be called the Born-Oppenheimer (BO) model. Similarly to Sec. II A, we introduce the Born-Oppenheimer adiabatic (BOA) eigenvalue problem

$$[\bar{H}_{\rm ad}(\bar{R})-\bar{U}_{\bar{\nu}}(\bar{R})]\bar{\Phi}_{\bar{\nu}}(\bar{\xi},\bar{\eta};\bar{R})=0. \tag{59}$$

This equation allows separation of the variables $\bar{\xi}$ and $\bar{\eta}$, which confirms the made above statement regarding exact separability of the HSA eigenvalue problem (19) in HSE coordinates in the limit (48). Seeking the solutions to Eq. (59) in the form

$$\bar{\Phi}_{\bar{\nu}}(\bar{\xi},\bar{\eta};\bar{R})=\bar{f}_{\bar{\nu}}(\bar{\xi};\bar{R})\bar{g}_{\bar{\nu}}(\bar{\eta};\bar{R}), \tag{60}$$

for the functions $\bar{f}_{\bar{\nu}}(\bar{\xi};\bar{R})$ and $\bar{g}_{\bar{\nu}}(\bar{\eta};\bar{R})$ one obtains

$$\left[2\frac{d}{d\bar{\xi}}(\bar{\xi}^2-1)\frac{d}{d\bar{\xi}}-\bar{R}\bar{a}(\bar{\xi})+\bar{U}_{\bar{\nu}}(\bar{R})(\bar{\xi}^2-1)-\tfrac{1}{2}\bar{A}_{\bar{\nu}}(\bar{R})\right]\bar{f}_{\bar{\nu}}(\bar{\xi};\bar{R})=0, \tag{61a}$$

$$\left[2\frac{d}{d\bar{\eta}}(1-\bar{\eta}^2)\frac{d}{d\bar{\eta}}-\bar{R}\bar{b}(\bar{\eta})+\bar{U}_{\bar{\nu}}(\bar{R})(1-\bar{\eta}^2)+\tfrac{1}{2}\bar{A}_{\bar{\nu}}(\bar{R})\right]\bar{g}_{\bar{\nu}}(\bar{\eta};\bar{R})=0. \tag{61b}$$

Apart from some inessential differences in notation and the definitions of the adiabatic potential $\bar{U}_{\bar{\nu}}(\bar{R})$ and the separation constant $\bar{A}_{\bar{\nu}}(\bar{R})$, Eqs. (61) coincide with equations describing the two center Coulomb problem in prolate spheroidal coordinates [26]. The differences are explained by our wish to demonstrate the continuous transition from Eqs. (28) to Eqs. (61) in the limit (48). The index $\bar{\nu}$ can be specified as

$$\bar{\nu}\equiv\nu|_{M\to\infty}=(n_{\bar{\xi}},n_{\bar{\eta}}),\quad n_{\bar{\xi}},n_{\bar{\eta}}=0,1,\ldots, \tag{62}$$

where $n_{\bar{\xi}}$ and $n_{\bar{\eta}}$ give the numbers of zeros of the solutions to Eqs. (61a) and (61b), respectively. The exact classification of the solutions to Eq. (59) by the *plane elliptic* quantum numbers $(n_{\bar{\xi}},n_{\bar{\eta}})$ naturally results in the limit (48) from the approximate classification of the solutions to Eq. (19) by the *hyperspherical elliptic* quantum numbers (n_ξ,n_η). However to comply with convention adopted in the two center Coulomb problem [26], in the following instead of $(n_{\bar{\xi}},n_{\bar{\eta}})$ we shall use the united atom quantum numbers. Thus the two lowest solutions to Eq. (59) corresponding to $(n_{\bar{\xi}},n_{\bar{\eta}})=(0,0)$ and $(0,2)$ will be denoted by $1s\sigma_g$ and $3d\sigma_g$, respectively. The eigenvalues of Eq. (59) converted to

$$\bar{W}_{\bar{\nu}}(\bar{R})\equiv W_\nu(R)|_{M\to\infty}=\frac{\bar{U}_{\bar{\nu}}(\bar{R})}{\bar{R}^2} \tag{63}$$

and the eigenfunctions normalized by

$$\langle\bar{\Phi}_{\bar{\nu}}|\bar{\Phi}_{\bar{\mu}}\rangle_{\rm BO}=\delta_{\bar{\nu}\bar{\mu}}, \tag{64}$$

where

$$\langle F\rangle_{\rm BO}\equiv\int_1^\infty d\bar{\xi}\int_{-1}^1 d\bar{\eta}(\bar{\xi}^2-\bar{\eta}^2)\times F(\bar{\xi},\bar{\eta}) \tag{65}$$

for an arbitrary $F(\bar{\xi},\bar{\eta})$, will be called the BOA potentials and channel functions, respectively. Without going into further details we note that the difference between $W_\nu(R)$ and $\bar{W}_{\bar{\nu}}(\bar{R})$ for large M is $\sim 1/M$.

We could continue this analysis of the BO model along the lines of Sec. II A and II B and obtain accurate results similar to that reported in Sec. II C. This development would be interesting in itself since though the BO model is known to be very useful and has many applications in studying bound states and various scattering processes in diatomic molecules, we are not aware of any its applications to calculating resonances. However this would not clarify the origin of the oscillations of $\Gamma(M)$ which is sought here. So instead we turn to perturbation theory which proves to be more helpful for the present purposes than accurate calculations.

B. Fermi-Fano-Feshbach perturbation analysis

We are interested in the lowest resonance state described by Eq. (54). As M grows, the motions of the heavy and the light particles represented in Eq. (54) by the variables $\bar{R}$ and $(\bar{\xi},\bar{\eta})$, respectively, become decoupled and the resonance width $\Gamma(M)$ vanishes. An adequate approach for treating such narrow resonances consists in first assuming the resonance state to be purely bound and then calculating its width by perturbation theory. Apparently the earliest recipe to implement this approach was given by Fermi's Golden Rule; later on, its physical content was enriched by Fano [27] and its consistent mathematical formulation was developed by Feshbach [28]. Following [27], the resonance width for the BO model (54) can be estimated as

$$\Gamma=2\pi\left|\int_0^\infty\left\langle\psi_{\mathcal{E}}\right|-\frac{1}{M}\frac{\partial^2}{\partial\bar{R}^2}+\frac{\bar{H}_{\rm ad}(\bar{R})}{\bar{R}^2}\left|\psi_0\right\rangle_{\rm BO}d\bar{R}\right|^2, \tag{66}$$

where ψ_0 and $\psi_{\mathcal{E}}$ are two approximate solutions to Eq. (54) corresponding to the same energy $E=\mathcal{E}$ and belonging to the discrete and continuous parts of the spectrum, respectively. Unless one goes into complexities associated with the rigorous definition of Feshbach's $\mathcal{P}$ and $\mathcal{Q}$ spaces [28], these functions remain undefined and can be chosen basing on *ad hoc* arguments. In the present situation the choice is rather evident. The resonance state of interest here is supported by

the second BOA channel $3d\sigma_g$. Accordingly, we define the bound state wave function ψ_0 by

$$\psi_0(\bar{R},\bar{\xi},\bar{\eta})=F_0(\bar{R})\bar{\Phi}_{3d\sigma_g}(\bar{\xi},\bar{\eta};\bar{R}), \tag{67}$$

where the radial function $F_0(\bar{R})$ satisfies the equation

$$\left(\frac{d^2}{d\bar{R}^2}+M[\mathcal{E}-\bar{W}_{3d\sigma_g}(\bar{R})]\right)F_0(\bar{R})=0, \tag{68a}$$

the boundary conditions

$$F_0(0)=F_0(\bar{R})|_{\bar{R}\to\infty}=0, \tag{68b}$$

and the normalization condition

$$\int_0^\infty F_0^2(\bar{R})d\bar{R}=1. \tag{68c}$$

The resonance position $\mathcal{E}$ is given by the lowest eigenvalue of Eqs. (68). The decay of the resonance can occur only into the lowest BOA channel $1s\sigma_g$. So similar equations defining the continuous energy wave function ψ_E read

$$\psi_E(\bar{R},\bar{\xi},\bar{\eta})=F_E(\bar{R})\bar{\Phi}_{1s\sigma_g}(\bar{\xi},\bar{\eta};\bar{R}), \tag{69}$$

where

$$\left(\frac{d^2}{d\bar{R}^2}+M[E-\bar{W}_{1s\sigma_g}(\bar{R})]\right)F_E(\bar{R})=0, \tag{70a}$$

$$F_E(0)=0,\quad F_E(\bar{R})|_{\bar{R}\to\infty}=\sqrt{\frac{M}{\pi K}}\sin[K\bar{R}+\delta], \tag{70b}$$

$$\int_0^\infty F_E(\bar{R})F_{E'}(\bar{R})d\bar{R}=\delta(E-E'). \tag{70c}$$

Here $K=\sqrt{M(E+1/2)}$ and δ is the phase shift for elastic scattering by the lowest BOA potential.

Substituting functions (67) and (69) into Eq. (66) and neglecting terms containing the second derivatives of the BOA channels with respect to $\bar{R}$, one obtains

$$\Gamma\approx\frac{8\pi}{M^2}\left|\int_0^\infty\frac{dF_{\mathcal{E}}(\bar{R})}{d\bar{R}}P_{1s\sigma_g,3d\sigma_g}(\bar{R})F_0(\bar{R})d\bar{R}\right|^2 \tag{71a}$$

$$\approx\frac{8\pi}{M^2}\left|\int_0^\infty F_{\mathcal{E}}(\bar{R})P_{1s\sigma_g,3d\sigma_g}(\bar{R})\frac{dF_0(\bar{R})}{d\bar{R}}d\bar{R}\right|^2, \tag{71b}$$

where

$$P_{1s\sigma_g,3d\sigma_g}(\bar{R})=|\langle\bar{\Phi}_{1s\sigma_g}|\partial/\partial\bar{R}|\bar{\Phi}_{3d\sigma_g}\rangle_{\mathrm{BO}}|$$
$$=\left|\frac{4\langle\bar{\Phi}_{1s\sigma_g}|\bar{\xi}(\bar{\xi}^2-\bar{\eta}^2)^{-1}|\bar{\Phi}_{3d\sigma_g}\rangle_{\mathrm{BO}}}{\bar{U}_{1s\sigma_g}(\bar{R})-\bar{U}_{3d\sigma_g}(\bar{R})}\right| \tag{72}$$

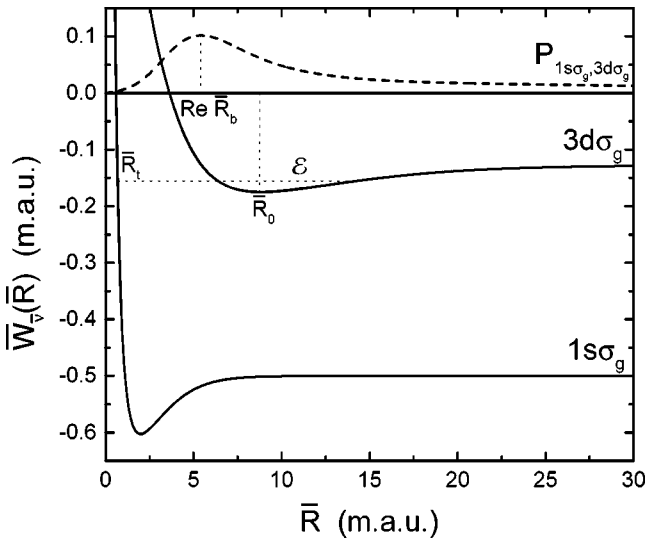

FIG. 4. Solid curves: two lowest adiabatic potentials $\bar{W}_\nu(\bar{R})$ for the Born-Oppenheimer model defined by Eqs. (59) and (63) as functons of the distance $\bar{R}$ between the identical particles defined by Eq. (50). Dashed curve: the nonadiabatic coupling between the states $1s\sigma_g$ and $3d\sigma_g$ defined by Eq. (72). $\bar{R}_0$ is the position of the minimum of the $3d\sigma_g$ potential; $\bar{R}_t$ is the turning point on the $1s\sigma_g$ potential for the energy $E=\mathcal{E}$; $\bar{R}_b$ is the closest to the real axis branch point connecting the sheets $1s\sigma_g$ and $3d\sigma_g$.

characterizes the strength of nonadiabatic coupling between the channels $1s\sigma_g$ and $3d\sigma_g$. The two formulas (71a) and (71a) differ by the second derivative terms neglected in the derivation. These terms contain an additional small factor $1/\sqrt{M}$, as compared with the first derivative term retained in Eqs. (71), and they should be neglected in the limit (48). Formulas (71a) and (71a) would be identical if function (72) were independent of $\bar{R}$.

Thus the procedure of calculating the resonance parameters $\mathcal{E}(M)$ and $\Gamma(M)$ in the present simplified treatment consists of the following steps: (i) constructing the two lowest BOA channels $1s\sigma_g$ and $3d\sigma_g$ and the nonadiabatic coupling between them (72) by solving Eqs. (61), and (ii) solving Eqs. (68) and (70) and calculating integrals (71) for different values of the mass-ratio M.

C. Results

The two lowest BOA potentials defined by Eqs. (59) and (63) relevant to discussing the resonance state of interest here are shown by the solid curves in Fig. 4. The abscissa in this figure coincides with that in Fig. 1 in the limit (48). The solid curves in Fig. 4 would be indistinguishable by the eye from that in Fig. 1 if plotted together, the difference being of the order $1/M\sim10^{-4}$ for the ppe system. The dashed curve in Fig. 4 represents function (72). The maximum of this function at $\bar{R}\approx5.4$ indicates the center of the region of strong nonadiabatic coupling between the involved states.

The resonance position $\mathcal{E}(M)$ obtained by solving Eqs. (68) is shown by the solid curves in Figs. 3(a) and 5(a). At small M, there is a considerable difference between the BO results and the accurate results reported in Sec. II C, as can be seen from Fig. 3(a). But this difference disappears in the

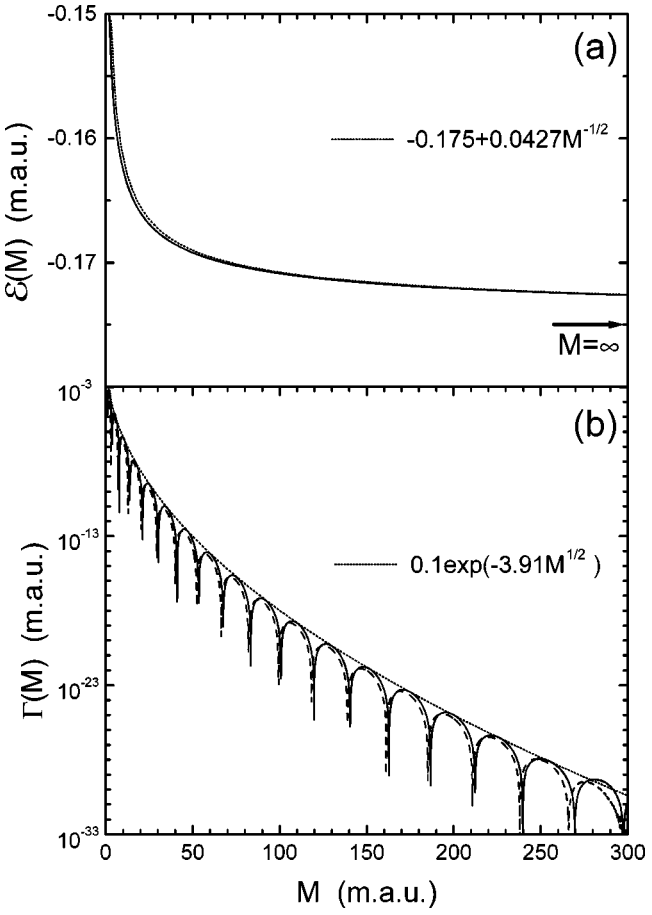

FIG. 5. Solid and dashed curves: results for the resonance position $\mathcal{E}(M)$ and width $\Gamma(M)$ obtained from the Born-Oppenheimer model, i.e., the same as the corresponding curves in Fig. 3, but for a wider interval of the mass-ratio M. Dotted curves: the semiclassical results obtained (a) from Eq. (75) and (b) by fitting the envelope of the Born-Oppenheimer results by that dictated by Eqs. (78) and (79).

limit (48) where the function $\mathcal{E}(M)$ defined by any of Eqs. (12), (54), and (68) approaches from above the minimum of the $3d\sigma_g$ BOA potential indicated by the arrows in Figs. 3(a) and 5(a) and given in the last entry of Table VII.

The resonance width $\Gamma(M)$ calculated according to Eqs. (71a) and (71b) is shown by the solid and dashed lines, respectively, in Figs. 3(b) and 5(b). As can be seen from Fig. 3(b), the BO results are very similar to the accurate results reported in Sec. II C. In both cases, the function $\Gamma(M)$ oscillates with an increasing period and decreasing envelope as M grows. A more detailed inspection of the figure shows that the periods and envelopes of these oscillations are rather close for the two cases. The main difference is that there is a phase shift between the oscillations which, however, also exists between the BO results obtained from Eqs. (71a) and (71b). Because now we calculate not $\Gamma(M)$ directly but the integrals in Eqs. (71), with the same intrinsic accuracy of calculations we can treat much smaller values of $\Gamma(M)$, thus being able to essentially extend the considered interval of M. In fact, with the present numerical procedure for solving Eqs. (68) and (70) which is based on the Numerov method we can extend our calculations up to $M=300$, which restricts the interval of M shown in Fig. 5. For even larger M, the integrands in Eqs. (71) oscillate too rapidly and the integrals become too small.

To summarize this section, the main conclusion which we would like to make here is that both the full-scale three-body Coulomb problem (12) and the BO model (54) obtained from Eq. (12) in the limit (48) lead to a very similar behavior of the resonance width $\Gamma(M)$. Therefore an explanation of the oscillations of $\Gamma(M)$ could be sought on the basis of Eq. (54). But the motion in $\bar{R}$ described by this equation, which couples the BOA channels and causes the decay of the resonance state, becomes *semiclassical* in the limit (48). Indeed, it is well known that the case of large masses is formally equivalent to the semiclassical situation $\hbar \to 0$: in both cases the coefficient of the second derivative term in the Schrödinger equation goes to zero. Thus an explanation of the oscillations of $\Gamma(M)$ should be sought in terms of semiclassical theory.

IV. QUALITATIVE DISCUSSION IN TERMS OF SEMICLASSICAL THEORY

The physics defining the existence of a resonance is quite different from and generally speaking much simpler than that defining its decay. For existence of a resonance state, as well as for existence of a bound state, certain quantization conditions imposed on a finite classically accessible region of configuration space must be satisfied. One can imagine a ball bouncing between walls in a box which gives a good intuitive picture of the underlying dynamics. On the other hand, decay of a resonance consists in passing from a finite to an infinite classically accessible region through a classically inaccessible barrier or a narrow classically accessible tunnel. Such passing or tunneling is beyond our intuition since we do not have classical laws of motion under the barrier. In this situation one often resorts to mathematical abstractions which help to restore an intuitive picture of the dynamics. One of such abstractions that proves to be essential in semiclassical theory is complex coordinate. Complexification of a coordinate implies analytical continuation of the corresponding potential energy function. For multichannel scattering problems this leads to the concept of adiabatic potential energy as a single multivalued analytical function of the scattering coordinate. Thus, for the three-body Coulomb problem (12), Eqs. (19) and (20) define the HSA potential $W(R)$ as a multivalued function of complex hyperradius R, and $W_\nu(R)$ give different branches of this function. Similarly for the BO model (54): Eqs. (59) and (63) define the BOA potential $\bar{W}(\bar{R})$ as a multivalued function of complex distance $\bar{R}$ between the particles 1 and 2, and $\bar{W}_\nu(\bar{R})$ give its different branches. The Riemann surface of such multivalued potential functions consists of as many sheets as many channels are in the problem. The sheets are connected by branch points forming a single potential energy surface. This surface is the key object in semiclassical theory providing an arena where the dynamics of the system takes place, while the dynamics itself is viewed as traveling over the surface. Such a viewpoint on the dynamics was pioneered in classical papers by Landau [29] and later on it has been used by many authors, especially in theory of chemical reactions [30–33]. In Ref. [34] this viewpoint was formulated as a research program and recently it has become known as Demkov's construction.

The Demkov's construction is currently receiving wide recognition via the framework of the hidden crossing theory proposed by Solov'ev [35], see Refs. [36–40]. Here, we shall use it for interpreting the oscillations of $\Gamma(M)$. But let us first return a step back and show how complex coordinates and a multivalued potential energy naturally arise in the theory.

Consider equations of Sec. III B in the limit (48). First we discuss the behavior of the resonance position $\mathcal{E}(M)$. Let $\overline{R}_0$ be the position of the minimum of the upper BOA potential shown in Fig. 4, and let

$$\overline{W}_{3d\sigma_g}(\overline{R})|_{\overline{R}\to\overline{R}_0}=v_0+v_2(\overline{R}-\overline{R}_0)^2+\cdots, \tag{73}$$

where $v_0=\overline{W}_{3d\sigma_g}(\overline{R}_0)$ and $v_2=\frac{1}{2}\overline{W}''_{3d\sigma_g}(\overline{R}_0)$. Substituting this expansion into Eq. (68a) and treating the higher terms perturbatively, in the lowest order we obtain

$$F_0(\overline{R})|_{M\to\infty}=\frac{(Mv_2)^{1/8}}{\pi^{1/4}}\exp[-\tfrac{1}{2}(Mv_2)^{1/2}(\overline{R}-\overline{R}_0)^2] \tag{74}$$

and

$$\mathcal{E}(M)|_{M\to\infty}=v_0+\left(\frac{v_2}{M}\right)^{1/2}. \tag{75}$$

Equation (75) gives the two leading terms of the expansion of $\mathcal{E}(M)$ in powers of $1/M^{1/2}$. The first term here is the value of the potential in the minimum, and the second term is a half of the vibrational quantum corresponding to oscillations near the minimum. We remark that these terms are the same for $\mathcal{E}(M)$ defined by Eqs. (12), (54), and (68); the difference arises in the term $\sim 1/M$. The numerical values of the coefficients in Eq. (73) obtained in the present calculations are $\overline{R}_0\approx 8.834\,164\,50$, $v_0\approx -0.175\,049\,036$, and $v_2\approx 0.182\,380\,852\times 10^{-2}$, which coincide in all digits quoted with the values given in [41]. The function defined by Eq. (75) is plotted by the dotted curve in Fig. 5(a). Except at small M, this curve is very close to the solid curve obtained by solving Eqs. (68) numerically.

Now we turn to the resonance width $\Gamma(M)$. Consider the three factors defining the integrands in Eqs. (71) separately. As follows from Eq. (74), function $F_0(\overline{R})$ is localized near the point $\overline{R}=\overline{R}_0$ having the width $|\overline{R}-\overline{R}_0|\sim 1/M^{1/4}$ which vanishes in the limit (48). For large M, an approximate semiclassical solution of Eqs. (70) in the region $\overline{R}>\overline{R}_t$ is given by

$$F_E(\overline{R})=\sqrt{\frac{M}{\pi K(\overline{R})}}\sin\left[\int_{\overline{R}_t}^{\overline{R}}K(\overline{R}')d\overline{R}'+\pi/4\right], \tag{76}$$

where

$$K(\overline{R})=\sqrt{M[E-\overline{W}_{1s\sigma_g}(\overline{R})]}, \tag{77}$$

and $\overline{R}_t$ is the turning point defined by $K(\overline{R}_t)=0$. Thus $F_E(\overline{R})$ oscillates with the period $\sim 1/M^{1/2}$ which for large M becomes smaller than the width of the function $F_0(\overline{R})$. The third factor, namely, the nonadiabatic coupling (72), is a slow varying function independent of M. Thus the integrands in Eqs. (71) are oscillatory functions with a bell-shaped envelope. The phase of these oscillations with respect to the envelope varies with M. This results in oscillations of the integrals (71), which technically explains the oscillations of $\Gamma(M)$. In fact, the integrals (71) become equal to zero for certain values of M which means zero resonance width $\Gamma(M)$, i.e., for such values of M the resonance state turns into bound state embedded into continuum. However this is an artifact of approximations assumed by Eqs. (66) and (71). As M grows, integrands in Eqs. (71) become highly oscillating functions and the integrals rapidly decrease. This causes essential difficulties in calculating the integrals numerically, which is a common problem in calculations of semiclassical matrix elements. A solution to this problem was given in [29] and consists in using the saddle point method. This requires to analytically continue the integrand into complex values of the integration variable, $\overline{R}$ in the case of Eqs. (71), and this is how complex coordinate comes into play. If both functions $F_0(\overline{R})$ and $F_E(\overline{R})$ in Eqs. (71) were substituted by semiclassical approximations like that given by Eq. (76), then it can be shown [29,43] that the saddle points of the integrand are defined by $\overline{W}_{1s\sigma_g}(\overline{R})=\overline{W}_{3d\sigma_g}(\overline{R})$, i.e., they are branch points of the BOA potential $\overline{W}(\overline{R})$. This is how one comes to the concept of a multivalued potential energy function.

Now we return to Demkov's construction and outline a physically transparent although somewhat speculative picture of the resonance decay dynamics. Suppose a state with the wave function (67) is prepared and placed into the upper potential well in Fig. 4. Because this wave function is not an exact solution of Eq. (54), the state will spread with time seeking a way to escape from the region where it is initially localized. But it cannot just jump from the upper to the lower potential curve, since this would cause an abrupt change of the wave function. So it descends continuously flowing down along the path on the Riemann surface of the BOA potential $\overline{W}(\overline{R})$ that starts from the real axis at $\overline{R}\approx\overline{R}_0$ on the upper sheet, goes around a branch point $\overline{R}_b$ connecting the sheets $1s\sigma_g$ and $3d\sigma_g$, and returns back to the real axis at $\overline{R}\approx\mathrm{Re}\,\overline{R}_b$ which approximately corresponds to the position of the maximum of the nonadiabatic coupling (72), but now on the lower sheet. Then there are two ways to proceed: reaching the real axis the flux can go to the right or to the left in Fig. 4. The former path leads directly to fragmentation region $\overline{R}\to\infty$, while choosing the latter path the flux firstly experiences reflection at the turning point $\overline{R}_t$ on the lower BOA potential, and only then goes to fragmentation region. The two paths lead to the same final state and their contributions to the outgoing flux at $\overline{R}\to\infty$ add coherently. This results in interference pattern seen as the oscillations of the resonance width $\Gamma(M)$.

Thus the oscillations of $\Gamma(M)$ can be interpreted as a result of interference between two paths of the decay of the resonance state. Let us provide some additional arguments to support this interpretation. Basing on the outlined above picture the functional structure of $\Gamma(M)$ can be specified as follows:

$$\Gamma(M)=a(M)e^{-\alpha(M)}\sin^2\phi(M). \tag{78}$$

The three factors in this formula have different origins and we discuss them separately.

The exponential factor in Eq. (78) arises from the fact that the semiclassical action accumulated along any path connecting two sheets of the Riemann surface of potential energy inevitably acquires imaginary part which is the larger the farther from the real axis lies the corresponding branch point $\overline{R_b}$. The presence of such exponential factor in the expression for probability of any nonadiabatic transition was first realized in [29]. This factor is the most important in Eq. (78) since it defines the order of magnitude of $\Gamma(M)$. The exponent $\alpha(M)$ is usually called the Massey parameter. In the present case it is a function of M which can be expanded as

$$\alpha(M)|_{M\to\infty}=\alpha_1 M^{1/2}+\alpha_0+\frac{\alpha_{-1}}{M^{1/2}}+\ \ldots. \tag{79}$$

Fitting the envelope of the BO results for $\Gamma(M)$ obtained from Eqs. (71) by the function $\propto e^{-\alpha_1\sqrt{M}}$, which corresponds to retaining only the first term in Eq. (79), we find $\alpha_1 \approx 3.91\pm 0.01$. The dotted curve in Fig. 5(b) shows this fit. One can see that, indeed, it very well reproduces the envelope of $\Gamma(M)$. Using this fit, the estimate of the resonance width for the molecular ion H_2^+ is $\Gamma\propto 10^{-73}$ a.u. meaning the lifetime $\propto 10^{48}$ years which is essentially longer than the age of universe. Thus the considered resonance state in H_2^+ and other molecular systems listed in the end of Table I can be with confidence treated as truly bound.

The oscillatory factor in Eq. (78) describes interference effects which always exist in the presence of turning points. The origin of this factor was first realized in [44] and $\phi(M)$ is called the Stueckelberg phase. This factor varies between 0 and 1 and in many situations, e.g., in calculations of total cross sections of nonadiabatic transitions, it can be replaced by its average value 1/2. However this is not always the case, and in situations where Stueckelberg phase is close to a multiple of π this factor may become essential. Thus destructive interference explains the small values of the S-wave cross sections for Ps formation in $e^+ + H$ collisions [39] and for muon transfer in the $dt\mu$ system [9,42]; destructive interference produces a dip in recombination probability for the reaction $^4He+{}^4He+{}^4He\to{}^4He+{}^4He_2$ [40]; and, eventually, it is destructive interference which causes the width $\Gamma(M)$ of the resonance discussed in this work to almost vanish at certain values of M. The Stueckelberg phase $\phi(M)$ is approximately equal to the real part of the difference between actions accumulated along two paths on the Riemann surface of potential energy, but it also includes an additional term, the so-called dynamical phase [30]. In the present case $\phi(M)$ can be expanded as

$$\phi(M)|_{M\to\infty}=\phi_1 M^{1/2}+\phi_0+\frac{\phi_{-1}}{M^{1/2}}+\ \ldots. \tag{80}$$

The solid [open] circles in Fig. 6 show the values of $M=M_n$ for which the integral (71a) [(71b)] vanishes. This happens when $\phi(M)=\pi n$, which defines M_n. Retaining the first two terms in Eq. (80) we obtain $M_n=(\pi n-\phi_0)^2/\phi_1^2$.

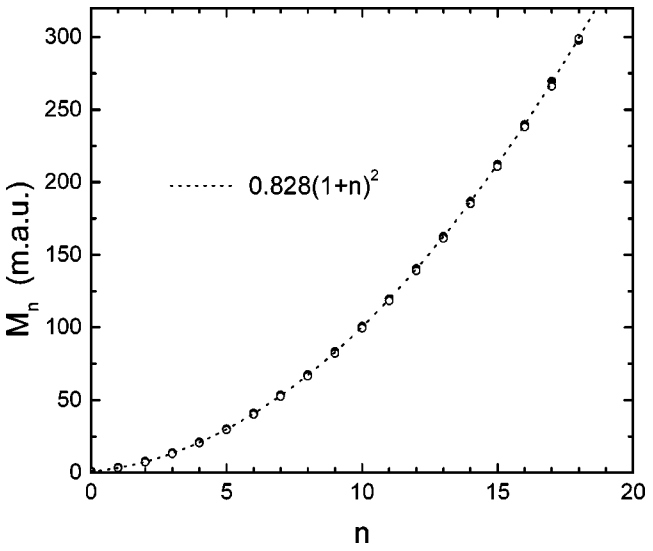

FIG. 6. M_n gives the position of the nth minimum of the resonance width $\Gamma(M)$ for the Born-Oppenheimer model. Solid and open circles—numerical results obtained from Eqs. (71a) and (71b), respectively. Dashed line is a fit to the numerical results according to Eqs. (78) and (80).

Fitting the numerical results for M_n by this function, we find $\phi_1\approx 3.45\pm 0.01$ and $\phi_0\approx -3.14\pm 0.01$. This fit is shown by the dotted curve in Fig. 6; it excellently reproduces the calculated values of M_n.

These two factors in Eq. (78) have a very general nature and are well understood. Thus, for example, the hidden crossing theory [35] should be able to yield the correct values of the Massey parameter $\alpha(M)$, as was demonstrated by a number of applications [36–40]. Perhaps it could also predict the values of the Stueckelberg phase $\phi(M)$, although in this case to achieve good quantitative agreement with accurate results will be more difficult becase of the dynamical phase which is not accounted for by the theory. Indeed, the calculations reported in [40] demonstrate strong dependence of the position of the dip in recombination probability on details of the theoretical model. It should be noted that in spite of this difficulty the hidden crossing theory seems to be the most appropriate framework for calculating $\alpha(M)$ and $\phi(M)$, at least it is hardly possible to do this staying on real coordinate axis, see the Appendix. The nature of the third factor in Eq. (78), i.e., the preexponent $a(M)$, is more subtle. It is defined by the Stokes' phenomenon and is not generally known, except for a few exactly solvable problems; see, e.g., a recent review [45]. In particular, this factor is not accounted for by the hidden crossing theory [35]. However $a(M)$ is usually a slow varying function as compared with the two other factors and replacing it by a constant does not produce any visible changes in log-scale plots such as Figs. 3(b) and 5(b).

To conclude this section, we have seen that semiclassical theory may be very helpful providing a transparent qualitative picture of the phenomenon. Whether it is capable of providing its quantitative description remains an open question to answer which goes beyond the scope of this paper.

V. SUMMARY OF RESULTS AND DISCUSSION

In this paper we have analyzed the lowest $^1S^e$ resonance state in a family of symmetric three-body Coulomb systems

as a function of the ratio M of the masses of the constituting particles. The results of accurate calculations by Siegert pseudostate method of the resonance position $\mathcal{E}(M)$ and width $\Gamma(M)$ in the interval $0 \leqslant M \leqslant 30$ are reported. This interval includes several realistic three-body Coulomb systems eep, eee^+, $pp\mu$, $dd\mu$, and $tt\mu$ for which the most accurate to date estimates of the resonance parameters have been obtained. But the principal finding of these calculations is that $\Gamma(M)$ oscillates as a function of M, which reveals an interference mechanism in the resonance decay dynamics. The perturbation analysis of a simplified model obtained from the three-body Coulomb problem in the limit $M \to \infty$ extends the considered interval of the mass-ratio up to $M = 300$, confirming that $\Gamma(M)$ continues to oscillate with an increasing period and decreasing envelope as M grows. Simultaneously it suggests that the mechanism of the oscillations could be interpreted in terms of semiclassical theory. The key role in such interpretation belongs to what is currently known as the Demkov's construction [34]. Decay of a resonance in this approach amounts to passing from the initial Riemann sheet of the adiabatic potential energy corresponding to the closed channel to a lower sheet corresponding to the open channel around a branch point connecting the sheets. Then the oscillations of $\Gamma(M)$ can be interpreted as a result of interference between two paths of the resonance decay, one of which goes directly to fragmentation region, while the other one first passes through the turning point on the lower sheet. In other words, the oscillations of $\Gamma(M)$ are a manifestation of the Stueckelberg phase [44] well known from analysis of different two-state models [30–33,45]. The dependences on M of the envelope of the function $\Gamma(M)$ and of the period of its oscillations obtained on the basis of this interpretation agree excellently with the present numerical results. This warrants more detailed study of the multivalued adiabatic potential energy for the three-body Coulomb problem and further development of the Demkov's construction in the framework of the hyperspherical method.

The discussed interference mechanism of the oscillations of $\Gamma(M)$ clearly has a very general nature. Similar oscillations should exist also in the dependence of resonance width on some other parameters, for example, the vibrational quantum number of the resonance state and the total angular momentum of the system. At the same time, variation of not any parameter can cause oscillations. Thus the width of the $2s^2\,{}^1S^e$ resonance state in two-electron atoms is known to be a monotonic function of the nuclear charge [46]. The oscillations found in this work raise a very interesting question of whether it is possible by varying some parameters of the system to achieve exactly *zero* resonance width, which would mean the existence of bound states embedded in the continuum of the three-body Coulomb problem. Note that there is not any general law that would forbid such a possibility. The oscillations also have a more practical implication: calculations of resonance width by approximate methods, like Fermi's Golden Rule, although giving the correct envelope for a wide range of some parameter can yield a completely wrong result for any its particular value.

We conclude by noting that although the mass-ratio M in realistic three-body Coulomb systems is not, of course, a continuous parameter, the results of this work can be applied also to charged excitons in semiconductors [47]. The effective masses of electrons and holes in such systems can vary considerably and the oscillations of $\Gamma(M)$ could be probably observed experimentally.

ACKNOWLEDGMENTS

O.I.T. thanks V.I. Osherov and H. Nakamura for many useful discussions on the different aspects of semiclassical theory. We would like to thank R. More for reading the manuscript. One of us (O.I.T.) gratefully acknowledges partial support from INTAS under Grant No. 97-11032, ''Theoretical Study of Exotic Atomic and Molecular Systems.''

APPENDIX: MISLEADING TEMPTATION

We suspect that reading Sec. IV a temptation might arise to derive a formula for the resonance width $\Gamma(M)$ in the limit (48) by substituting functions (74) and (76) into Eqs. (71) and estimating the integrals. Indeed, there is no doubt that function (74) provides a very good point-to-point approximation to the exact solution of Eqs. (68) for sufficiently large M. The same holds for function (76) in respect to Eqs. (70), at least in the vicinity of the point $\bar{R} = \bar{R}_0$ where integrals in Eqs. (71) seem to accumulate. The nonadiabatic coupling (72) is a slow varying function and can be replaced by the constant $P_0 = P_{1s\sigma_g,3d\sigma_g}(\bar{R}_0)$. Acting this way, one would obtain for $\Gamma(M)$ formula of the form (78), where the leading terms in the expansions of the preexponent factor $a(M)$, the Massey parameter $\alpha(M)$, and the Stueckelberg phase $\phi(M)$ for large M are given by

$$a(M) = 16P_0^2 \frac{\pi^{1/2} K_0}{v_2^{1/4}} \frac{1}{M^{5/4}} \approx \frac{0.29}{M^{3/4}}, \tag{A1}$$

$$\alpha(M) = \frac{K_0^2}{(M v_2)^{1/2}} \approx 7.64 M^{1/2}, \tag{A2}$$

$$\phi(M) = \int_{\bar{R}_t}^{\bar{R}_0} K(\bar{R}')\, d\bar{R}' \approx 4.82 M^{1/2}, \tag{A3}$$

where $K(\bar{R}) = \sqrt{M[v_0 - \bar{W}_{1s\sigma_g}(\bar{R})]}$ and $K_0 = K(\bar{R}_0)$. Comparing this equations with expansions (79) and (80) one can see that the values of the parameters $\alpha_1 \approx 3.91$ and $\phi_1 \approx 3.45$ obtained from fitting the numerical results, as discussed in Sec. IV, are quite different from the values $\tilde{\alpha}_1 \approx 7.64$ and $\tilde{\phi}_1 \approx 4.82$ that follow from Eqs. (A2) and (A3). This is not surprising because in order to obtain correct values of the exponentially small integrals (71) functions (74) and (76) must approximate the exact solutions of Eqs. (68) and (70) with exponentially small error, which is not the case. Thus the discussed temptation is misleading and should be avoided.

[1] A. J. F. Siegert, Phys. Rev. **56**, 750 (1939).
[2] O. I. Tolstikhin, V. N. Ostrovsky, and H. Nakamura, Phys. Rev. Lett. **79**, 2026 (1997).
[3] O. I. Tolstikhin, V. N. Ostrovsky, and H. Nakamura, Phys. Rev. A **58**, 2077 (1998).
[4] O. I. Tolstikhin, S. Watanabe, and M. Matsuzawa, Phys. Rev. Lett. **74**, 3573 (1995).
[5] O. I. Tolstikhin, S. Watanabe, and M. Matsuzawa, in *The Physics of Electronic and Atomic Collisions*, Proceedings of the XIX International Conference, Whistler, Canada, 1995, edited by L. J. Dubé *et al.*, AIP Conf. Proc. No. 360 (AIP, Woodbury, NY, 1996), p. 887.
[6] O. I. Tolstikhin, S. Watanabe, and M. Matsuzawa, J. Phys. B **29**, L389 (1996).
[7] O. I. Tolstikhin, S. Watanabe, and M. Matsuzawa, Phys. Rev. A **54**, R3705 (1996).
[8] O. I. Tolstikhin, V. N. Ostrovsky, and H. Nakamura, Phys. Rev. Lett. **80**, 41 (1998).
[9] O. I. Tolstikhin and C. Namba, Phys. Rev. A **60**, 511 (1999).
[10] R. Madden and K. Codling, Phys. Rev. Lett. **10**, 516 (1963).
[11] M. S. Lubell, Can. J. Phys. **74**, 713 (1996).
[12] A. Carrington, I. R. McNab, and C. A. Montgomerie, J. Phys. B **22**, 3551 (1989).
[13] Particle Data Group, *Particle Physics Booklet* (Springer, New York, 1998).
[14] O. I. Tolstikhin and H. Nakamura, J. Chem. Phys. **108**, 8899 (1998).
[15] K. Nobusada, O. I. Tolstikhin, and H. Nakamura, J. Chem. Phys. **108**, 8922 (1998); J. Phys. Chem. A **102**, 9445 (1998); J. Mol. Struct.: THEOCHEM **461-462**, 137 (1999); G. V. Mil'nikov, O. I. Tolstikhin, K. Nobusada, and H. Nakamura, Phys. Chem. Chem. Phys. **1**, 1159 (1999).
[16] F. T. Smith, J. Chem. Phys. **31**, 1352 (1959).
[17] L. M. Delves, Nucl. Phys. **B9**, 391 (1958/59); **B20**, 275 (1960).
[18] A. Kuppermann, Chem. Phys. Lett. **32**, 374 (1975).
[19] F. T. Smith, Phys. Rev. **120**, 1058 (1960).
[20] J. Macek, J. Phys. B **1**, 831 (1968).
[21] U. Fano, Phys. Rev. A **24**, 2402 (1981); Rep. Prog. Phys. **46**, 97 (1983).
[22] C. D. Lin, Adv. At. Mol. Phys. **22**, 77 (1986); Rep. Prog. Phys. **257**, 1 (1995).
[23] D. O. Harris, G. G. Engerholm, and W. D. Gwinn, J. Chem. Phys. **43**, 1515 (1965); A. S. Dickinson and P. R. Certain, *ibid.* **49**, 4209 (1968); J. C. Light, I. P. Hamilton, and J. V. Lill, *ibid.* **82**, 1400 (1985).
[24] Y. K. Ho, Phys. Lett. A **102**, 348 (1984).
[25] S. Hara and T. Ishihara, Phys. Rev. A **40**, 4232 (1989).
[26] I. V. Komarov, L. I. Ponomarev, and S. Yu. Slavyanov, *Spheroidal and Coulomb Spheroidal Functions* (Nauka, Moscow, 1976).
[27] U. Fano, Nuovo Cimento **12**, 156 (1935); Phys. Rev. **124**, 1866 (1961).
[28] H. Feshbach, Ann. Phys. (N.Y.) **5**, 357 (1958); **19**, 287 (1962).
[29] L. Landau, Phys. Z. Sowjetunion **1**, 88 (1932); **2**, 46 (1932).
[30] E. E. Nikitin and S. Ya. Umanskii, *Theory of Slow Atomic Collisions* (Springer-Verlag, Berlin, 1984).
[31] M. S. Child, *Semiclassical Mechanics with Molecular Applications* (Clarendon, Oxford, 1991).
[32] E. S. Medvedev and V. I. Osherov, *Radiationless Transitions in Polyatomic Molecules* (Springer-Verlag, Berlin, 1995).
[33] H. Nakamura, in *Dynamics of Molecules and Chemical Reactions*, edited by R. E. Wyatt and J. Z. H. Zhang (Marcel-Dekker, NY, 1996), p. 473.
[34] Yu. N. Demkov, in *The Physics of Electronic and Atomic Collisions, ICPEAC-V. Invited Papers*, edited by L. M. Branscomb (Nauka, Leningrad, 1967), p. 186.
[35] E. A. Solov'ev, Usp. Fiz. Nauk **157**, 437 (1989) [Sov. Phys. Usp. **32**, 228 (1989)]; in *The Physics of Electronic and Atomic Collisions*, Ref. [5], p. 471.
[36] J. H. Macek and S. Yu. Ovchinnikov, Phys. Rev. A **50**, 468 (1994); **54**, 544 (1996).
[37] R. K. Janev, J. Pop-Jordanov, and E. A. Solov'ev, J. Phys. B **30**, L353 (1997).
[38] L. I. Ponomarev and E. A. Solov'ev, Pis'ma Zh. Éksp. Teor. Fiz. **68**, 9 (1998) [JETP Lett. **68**, 7 (1998)].
[39] S. J. Ward, J. H. Macek, and S. Yu. Ovchinnikov, Phys. Rev. A **59**, 4418 (1999).
[40] E. Nielsen and J. H. Macek, Phys. Rev. Lett. **83**, 1566 (1999).
[41] M. Shafi and C. L. Beckel, J. Chem. Phys. **59**, 5294 (1973).
[42] V. N. Ostrovsky, private communication.
[43] L. D. Landau and E. M. Lifshitz, *Quantum Mechanics (Non-Relativistic Theory)* (Pergamon, Oxford, 1977).
[44] E. C. G. Stueckelberg, Helv. Phys. Acta **5**, 369 (1932).
[45] S. F. C. O'Rourke, B. S. Nesbitt, and D. S. F. Crothers, Adv. Chem. Phys. **103**, 217 (1998).
[46] Y. K. Ho, Phys. Rev. A **23**, 2137 (1981).
[47] G. Munschy and B. Stébé, Phys. Status Solidi B **64**, 213 (1974).